BOULDER, COLORADO

July 19, 1965 PM # 135

G. M. Hidy and E. J. Plate

Wind Action on Water Standing in a Laboratory Channel

NCAR PREPRINT-MEMO

This form is designed for unrestricted use as a title page on manuscripts and draft copies, as well as the final versions of memoranda. Because these memos are intended for initial documentation and communication within NCAR, they may be quite informal and they may be changed without notice. Technical notes and other formal reports should be coordinated with the NCAR Publications Office.

* * Call the NCAR Library to obtain a PM # for your preprint-memos.
Also - Reprint - Journal of Fluid Mechanics - Vol. 26 - '66

NATIONAL CENTER FOR ATMOSPHERIC RESEARCH

BOULDER, COLORADO

* *

Date July 19, 1965 PM # 135

Author(s): G. M. Hidy and E. J. Plate

Title: Wind Action on Water Standing in a Laboratory Channel

No. of pages: 40

Summary: A systematic investigation of air and water motion associated with water initially standing in a channel is described. Several interesting features of the flow of the two fluids are discussed in the light of recent theoretical studies.

Author signature(s): G. M. Hidy

Group or program: 2130

(If applicable)

Formal publication plans: Submitted to J. Fluid Mech.

Distribution notes: (Air-Water Interaction list of Hidy)

WIND ACTION ON WATER STANDING IN A LABORATORY CHANNEL

G. M. Hidy
National Center for Atmospheric Research
Boulder, Colorado

and

E. J. Plate
Fluid Dynamics and Diffusion Laboratory
Colorado State University
Fort Collins, Colorado

ABSTRACT

The processes of wave and current development resulting from wind action on initially standing water have been investigated in a wind-water tunnel. The mean air flow over wavy water was examined along with the variation of several properties of the water motion with fetch, water depth, and wind speed. Measurements of phase speed and length of significant waves, the standard deviation of the water surface, the average surface drift, the autocorrelation of surface displacement and the frequency spectra of the wind waves are reported. The experimental results indicate that (a) the air motion in the channel follows a three dimensional pattern characteristic of wind tunnels of rectangular cross-section; (b) the wind waves generated in the channel travel downstream at approximately the same phase speed as gravity waves of small amplitude, provided the effect of the drift current is taken into account; (c) the average drag coefficients for the action of the wind on the water surface increase with increasing wind speed, and these data are essentially the same as the results of previous investigators; (d) the autocorrelations of surface displacement and frequency spectra are consistent with the visual observations that the wind waves in the channel consist of nearly regular primary waves on which are superimposed smaller ripples; (e) energy in the high frequency range in the spectra tends to approach an equilibrium distribution rather quickly while the lower frequency components initially grow exponentially with increasing fetch but, later, tend to reach a state of equilibrium; and (f) a similarity shape for the frequency spectra developed.

I. INTRODUCTION

In spite of a long history of effort devoted to the air-water interaction problem, the basic knowledge of the mechanisms for transport processes near the boundary between the two fluids has developed rather slowly. A variety of theoretical and experimental studies have been reported in the literature but, because of the complexities of the physical processes involved, the detailed nature of the interaction remains inadequately understood.

Many of the experimental studies of air-water interaction have been undertaken on lakes or on the ocean where the conditions of the fluids are highly variable in time and space. These investigations have contributed significantly to the knowledge of the atmosphere and the sea. However, their usefulness in elucidating the fundamental physics of the exchange processes occurring between the two fluids is limited. Therefore, it seems necessary to undertake more studies under controlled conditions in the laboratory to gain new insights into the mechanisms of transport across the air-water boundary.

Ursell (1956) has reviewed the fundamental laboratory experiments dealing with air-water interaction that were carried out before 1954. Since the publication of Ursell's paper, a number of new investigations have been reported which include those of Cox (1958), Wiegel and coworkers (e.g., Wiegel (1961)), Fitzgerald (1963), Kunishi (1963), Schooley (1963), Holmes (1963), and Hanratty and coworkers (e.g., Cohen and Hanratty (1965)). These laboratory investigations have explored a number of special problems associated with flow in the two phase system such as the mean properties of the waves, the mean air motion, or the nature of the wind driven drift current in the water. With the exception of Cohen and Hanratty's work, the experiments were not designed specifically to verify theoretical conclusions. In the spirit of most earlier experimental work, this study will deal in a unified way with both the air motion and the water motion. In addition, a number of interesting features of the two fluid system will be discussed in the light of the results of recent theoretical studies.

Properties of the Fluid Motion. When air moves at moderate velocities over water, a drift current develops and small waves are generated on the liquid surface. A schematic picture of the development of combined air and water motion along with the growth of waves in a channel is shown in Fig. 1. Some of the properties of fluid motion examined in this study are indicated in this drawing. The coordinate system is indicated so that x is the distance downstream, and z is the vertical direction. The mean water surface is given by z = d while the surface displacement from this level is denoted as ξ. The fetch F denotes the distance from the leading edge of the water to a particular point somewhere downstream. In terms of a two dimensional model, the velocity distribution in the water is u(z), and the drift at the water surface is u_o. The air flow is given by U(z'), where U_∞ denotes the air velocity at approximately 20 cm above the mean water surface, and z' = (z - d). The wave length $\bar{\lambda}$ and the phase speed $\bar{c}$ denote properties of significant waves.

For the purpose of this study, significant waves will refer to the larger, regular waves observed at a given fetch. In general, smaller ripples are superimposed on the larger disturbances (See, for example, Plate I).

In this paper, a number of experimental results are discussed which refer to the mean air and water flow as indicated in Fig. 1. Measurements of the statistical properties of the wind generated waves, including the autocorrelation of the surface displacement and spectral density functions, are examined in the light of other characteristics of the fluid motion.

2. EXPERIMENTAL EQUIPMENT AND PROCEDURE

The experiments were conducted in the wind-water tunnel at Colorado State University. This facility, shown schematically in Fig. 2, consists of a tunnel or a closed channel 0.61 m wide by 0.76 m high whose plexiglass test section has a length of about 12 m. During operation, the maximum depth of water is approximately 15 cm. Air is sucked through the tunnel at velocities up to 18 mps by a large axial fan at the outlet. The inlet cone is designed to give a 4/1 contraction ratio. Two fine mesh screens are placed in the inlet cone. Honeycombs are placed just upstream of the outlet diffuser to minimize the axial rotation in the air induced by the fan. Sloping beaches are placed at the inlet and the outlet to prevent the reflection of waves. The "beaches" are constructed

of aluminum honeycomb. The inclines are shaped in such a way that as smooth as possible a transition could be affected in the air-water flow. In this study, the bottom of the tunnel was smooth.

The air flow through the tunnel was measured by a pitot-static tube placed on a carriage in conjunction with a capacitative pressure transducer. The probe could be positioned anywhere in the section of the tunnel from the bottom to a level about 10 cm from the top.

The pressure gradient of the air and the depth of the water were measured every four feet down the tunnel with piezometer taps connected to a set of manometers.

Phase speeds and lengths of waves were determined from photographs taken with a movie camera. The length for successive waves was measured from the movies by comparing the distance between crests with a ruler in the picture. The phase velocities of waves referred to a fixed point were estimated by measuring from adjacent frames the distance traveled by a given crest during the time between successive frames. Time intervals between frames were read from a timer that was shown on the film.

To measure the change in the height of the water, a capacitance probe was used which is similar to Tucker and Charnock's (1955). This probe consisted of a 34 gauge magnet wire stretched vertically along the center line of the cross-section of the tunnel. These wires were placed at 1.2 m intervals downstream from the inlet of the tunnel. The wire itself and the water serve as the two plates of a condenser, and the insulation material (Nyclad) on the wire provides the dielectric medium. The capacitance between the wire and the water was measured with an AC excited bridge; the unbalance voltage from the bridge was linearized, amplified and rectified so that a DC output voltage was obtained which was proportional to the water depth. The output signal was fed to an oscillograph where the gauge response was continuously recorded during a run. The capacitance bridge-oscillograph combination was calibrated to give a recorded amplitude linearly proportional to the (varying) water depth with a flat response to frequency ($\pm$ 1%) up to approximately 30 cps.

From the continuous records of the surface displacement, data were read off at equal intervals of 0.025 sec. These data were used for obtaining values of standard deviation σ of the surface displacement, the

autocorrelations $R(\tau)$ of the surface displacement, and the spectral density function $\Phi(f)$. The computations were carried out on the NCAR-CDC 3600 computer.

It was not possible to obtain the vertical velocity distribution in the water. However, the surface velocity of the water u_o was measured by placing a small slightly buoyant particle on the water and observing the time required for it to move past fixed stations downstream. Values of the surface velocity could then be calculated from the intervals of distance of travel and the time of passage.

In this study, attention was centered on the measurement of the properties of water waves under conditions of steady (mean) air motion. In order to attain steady conditions in the air flow, the wave development, and the set up of water in the tunnel, the fan was started about 15-20 minutes before the properties of the fluid flow were to be measured. After this time interval, the photographs, the pitot tube measurements, and the wave amplitude data were taken, and a sample of a wave train corresponding to the passage of 100-200 waves was obtained for a given run.

Observations of wave development were taken for several different conditions. For the condition of water initially standing on a smooth bottom, air velocities, taken 20 cm above the water surface, were varied from 0 to 15 mps, and the depth of water was changed from 2.5 to 10 cm. The properties of fluid motion in these cases were observed at distances of approximately 1.8 meters to 12 meters from the leading edge of the water.

3. THE AIR FLOW OVER THE WATER

Since the air is forced by the fan through the wind tunnel of approximately constant cross section, a pressure gradient develops in the downstream direction. The pressure in the air p_A was found to vary approximately linearly with fetch through the channel. Typical values of the pressure gradient in cm water per cm as measured in the last 6 meters of the channel are shown in Fig. 3. The pressure gradient was found to increase with wind speed, and with depth of the water.

Velocity Distribution in the Air. Measurements of the mean horizontal air motion in the vertical direction and across the channel were taken at several sections for U_∞ from 6 mps to about 14 mps. Typical

data for vertical profiles along the center section of the channel are shown in Fig. 4A. The vertical profiles of U(z') indicate that the air flow generally develops a behavior characteristic of turbulent flow in a boundary layer over roughened surfaces.

The vertical profiles for the air velocity taken for increasing fetch along the centerline of the tunnel were found to be approximately proportional to $[(z - d)/\delta]^{1/n}$, where δ is the thickness of the boundary layer. Near the leading edge of the water surface, $n \approx 7$. However, over a wide range of F, and for $6.1 < U_\infty < 13.6$ mps, the data taken in the channel fit an exponential rule where $n \approx 4.5$. The shape of velocity profiles corresponding to this value of n is frequently found in wind tunnel data for flow over moderately rough surfaces.

Typical measurements of the horizontal distribution of velocity are shown in Fig. 4B. These data are representative of flow in wind tunnels of rectangular cross-section. It is interesting to note that the boundary layers associated with the side walls can become rather thick. This thickening had no apparent effect, however, on the development of significant waves in the channel. As shown in Plate I, the waves still exhibited a nearly linear crest moving approximately normal to the mean wind direction.

The lines of constant air velocity plotted for a given cross-section reveal an interesting feature of the channel flow as shown in Fig. 5. Because of a secondary circulation in the tunnel, the lines of constant velocity are squeezed down in the corners of the cross-section. This has been observed previously for flow in rectangular ducts (e.g., Schlichting (1960)). However, the effect appears to become somewhat more pronounced when fluid flows over a moving boundary in the CSU channel.

The three dimensional structure of the air flow does not visibly affect the waves generated on the water surface. However, the pressing of the air moving at higher speeds down along the walls seems to be transmitted to the horizontal velocity in the water. Measurements of the horizontal distribution of velocity in moving water indicated two maxima developing just underneath the "ears" of the constant velocity curves drawn in Fig. 5. Hence, strictly speaking, the local velocity in the air and in water should be analyzed for variation over the entire cross-section. However, for the purposes of this discussion the motion

of the air and the water will be treated as two dimensional. That is, only a narrow, uniform region of fluid flow near the center of the channel will be considered.

Shearing Stress on the Water Surface. An important parameter for measuring the action of the wind on the water is the shearing stress exerted by the air on the water surface, τ_s. The average shearing stress can be estimated from the equation for the momentum balance on the body of water standing in the channel. Assuming that the fluid motion is two dimensional, the average of the sum of the surface stress τ_s and the stress τ_b at the channel bottom is:

$$\overline{(\tau_s + \tau_b)} = d\rho_w g \left[S_w + \frac{1}{\rho_w g} \left(\frac{dp_A}{dx} \right) \right] , \qquad (3.1)$$

where S_w is the slope of the water surface, and d is the water depth at a fetch F. Since Eq. (3.1) is not sufficient to calculate the surface stress, a second relation is needed to separate $\bar{\tau}_s$ and $\bar{\tau}_b$.

An equation between the surface stress and the bottom stress was found by Keulegan (1951) for laminar flow in the water. Keulegan's result expressed $\bar{\tau}_s / \bar{\tau}_b$ as 1.5. For turbulent motion in the water, however, Francis (1951) indicated that $\bar{\tau}_b$ is very small compared to $\bar{\tau}_s$. Keulegan, on the other hand, estimated that the ratio $\bar{\tau}_s / \bar{\tau}_b$ for turbulent motion is about 1.25. More recent evidence of Baines and Knapp (1965) indicates that $\bar{\tau}_b$ is less than 10% of $\bar{\tau}_s$ for cases of turbulent channel flow. Another attempt to separate the bottom stress from the surface stress has been made by Goodwin (1965), who considered a momentum balance on the body of air above the water. His results are too scattered to be conclusive, but there is an indication that $\bar{\tau}_b$ is again much smaller than $\bar{\tau}_s$ for turbulent flow in the water.

Ursell (1956) has also criticized Eq. (3.1) in that it neglects the effect of changes in water velocity resulting from variation in depth. Goodwin (1965) calculated the correction to Eq. (3.1) given by Ursell to account for this effect. He found that for experiments in the Colorado State University channel, the error in total shearing stress would be the order of 1% if the effect of varying water depth were included. Therefore, for the purposes of this study, $\bar{\tau}_s$ has been estimated from Eq. (3.1) by disregarding the contribution of $\bar{\tau}_b$ and the effect of variation in water depth.

The data for $\bar{\tau}_s$ are presented with corresponding results of Keulegan (1951) and Fitzgerald (1962) in Fig. 6. The shearing stress is presented in the form of an average coefficient of shearing stress:

$$\bar{c}_s = \bar{\tau}_s / \rho_A \, U_{avg}^2 \quad , \tag{3.2}$$

where U_{avg} is the air velocity averaged over the cross-section of the tunnel.[1]

---

[1] For use as a reference velocity, the values of U_{avg} were calibrated against the value of U_∞ taken at a fetch of 9 meters ($U_{avg} \approx 0.80\, U_\infty$).

The results of our experiments, taken at several water depths, show some scatter, but they are quite close to the experimentally derived curves of both Keulegan and Fitzgerald. The systematic deviation of our data for the depth of 12.7 cm is probably not real because the slope of the water surface was very small in this case. Measurements of the surface slope S_w provide the largest source of error in Eq. (3.1).

As observed by other investigators, the average drag on the water surface in channels increases approximately linearly with wind speed over a fairly wide range of wind speed. There may be a tendency for the drag to increase more rapidly than the linear value at the highest values of U_{avg}. However, the data in Fig. 6 cannot be considered conclusive.

Local values of the coefficient of shearing stress can be estimated from the growth of the boundary layer in the air using the momentum integral technique described by Schlichting (1960). The relation for c_s by this method is:

$$c_s = \frac{\tau_s}{\rho_A U_\infty^2} = \frac{1}{U_\infty^2} \left[\frac{d(U_\infty^2 \, \Theta)}{dx} - \frac{\delta^*}{\rho_A} \frac{dp_A}{dx} \right] \tag{3.3}$$

where δ^* is the displacement thickness:

$$\delta^* = \frac{1}{U_\infty} \int_d^{z''} (U_\infty - U)\, dz' \quad , \tag{3.4}$$

is the momentum thickness:

$$\Theta = \frac{1}{U_\infty^2} \int_d^{z''} U\,(U_\infty - U)\, dz' \quad . \tag{3.5}$$

and z'' is the value of z' where $U = U_\infty$.

To accurately obtain values of c_s from Eq. (3.3), the slope of $U_\infty^2 \Theta$ and the values of δ^* must be well established. The contribution of $(U_\infty - U)$ to the integrals in Eqs. (3.4) and (3.5) depends strongly on the region of the vertical profile where the curvature is greatest. In our measurements, this is poorly defined because the curving portion of U(z') lies too close to the water for accurate measurement with the fixed probe. Thus, the use of Eq. (3.3) with Eqs. (3.4) and (3.5) may be expected to give only a first approximation in estimating the coefficient c_s.

In addition to the problem of using the experimental data in Eqs. (3.4-3.5) the application of a definition for a proper air velocity must be considered. Eq. (3.3) applies to flow over a solid boundary. When the boundary is moving and waves are superimposed on this motion, the air speed relative to fixed coordinates may be an incorrect estimate for U(z'). At least two other systems of velocity coordinates can be used. The air velocity relative to the surface drift may be a better system, or as Benjamin (1959) has noted, the motion relative to the phase speed may be better than the fixed system of reference. Introduction of either one of these reference velocities will affect the definitions of δ^*, Θ, δ, and consequently, c_s.

In spite of these difficulties, it is useful as a first approximation to apply Eq. (3.3) for evaluating c_s. Calculations of the local drag coefficients based on the data for U(z') were made, and some typical results for δ^*, $U_\infty^2 \Theta$, c_s are shown in Fig. 7. The results indicate that c_s decreases somewhat with fetch, but tends to increase with wind speeds higher than used for the data in Fig. 7. The decrease with fetch is typical of the variation in c_s in the context of a growing boundary layer over a solid surface.

Using the result of calibration, $U_{avg} = 0.80\, U_\infty$, c_s can be estimated from the data for c_s. Seven values at 1.5 meter intervals along the smoothed curves for c_s and U_∞ were chosen and averaged for two cases. The resulting values of c_s estimated in this way for two cases are shown with the other data in Fig. 6. The average coefficient of shearing stress evaluated in these two different ways check satisfactorily. This result also provides consistent evidence, on the one hand, that the bottom shear is a small part of the total shear evaluated in Eq. (3.1) over the range of $4 < U_{avg} < 7$ mps. On the other hand, this check suggests that the

procedure used for flow over solid boundaries may be adequate for describing the features of air flow over waves moving much slower than the air.

Similarity in the Horizontal Velocity. It is of interest to see if the mean velocity profiles along the center line of the channel can be correlated in terms of the mean shearing stress at the water surface. Similarity for flow in boundary layers can be expressed in terms of the velocity defect rule (See, for example, Townsend (1956)), where

$$U_\infty - U(z') = \frac{U^*}{K} f(z'/\delta) \tag{3.6}$$

U^* is the friction velocity

$$U^* = (\tau_s / \rho_A)^{1/2} , \tag{3.7}$$

K is Karman's Constant, and f is a "universal" function of the dimensionless length, z'/δ.

The data for the vertical distribution of air velocity along the center line have been computed in the form of Eq. (3.6) using $\overline{\tau}_s$ from Eq. (3.2) in Eq. (3.7). The velocity curves are shown in Fig. 8. There exists a rough similarity between the data calculated in this way, but the correlation is not as good as is observed for some cases of flow in boundary layers. This result is not surprising since, strictly speaking, the local value of U^* should be used in Eq. (3.6) and there are uncertainties in the evaluation of δ.

4. PROPERTIES OF THE WIND INDUCED WATER MOTION

Wind Generated Waves. Over a wide range of air flow which follows the patterns described in Sec. 3, only small gravity waves and capillary ripples were generated on the water standing in the channel. Although the air reached speeds greater than 14 mps, breaking of waves, in the sense of forming white caps, was not observed. At high air velocities droplets of spray were observed being shed from crests of the larger waves, but the waves did not become sharp crested as seen in "fully developed" seas.

Up to wind speeds of about 3 mps, taken about 20 cm above the water, no waves appeared on the water surface. However, very small oscillations

of the entire water surface could be observed in this range of air flow by watching variations in reflected light on the water. Above 3 mps, ripples began to form near the leading edge of the water. These small disturbances had wave lengths of 1-3 cm. Their direction of propogation was primarily normal to the wind direction. As the wind speed increased, the ripples initially present became larger in amplitude and height. Under the action of the steady air motion, the waves traveled downstream at an increasing speed, growing in amplitude and length. For wind speeds in the range U_∞ = 3-6 mps, significant waves were observed to run with crests approximately normal to the wind direction, with smooth windward surfaces, and rippled leeward surfaces. Above 6 mps, capillary ripples were noted on both the windward and the leeward sides of the significant waves. At any given point downstream from the inlet, groups of 5-20 small gravity waves of nearly the same period passed by. These groups were separated by relatively calm regions of small ripples having varied periods. The existence of groups of waves separated by relatively calm water is probably related to interference between different components of the wave train giving an appearance of "beats".

Typical examples of the development of waves with wind speed are shown in Plate I. These observations are taken at a fetch of about 8 meters. Note here the presence of the smaller ripples on the larger regular waves at higher wind speeds, as well as the nearly symmetrical appearance of the shapes of some waves.

Typical orders of magnitude of the observed wave lengths and phase speeds for significant waves generated at say $U_\infty \approx$ 6 mps were 10 cm, and 40 cm/sec. Since the phase speeds were much smaller than the wind speeds, it is expected qualitatively that the waves generated under our laboratory conditions were closely related to the action of the air in the layer near the water surface. Within the framework of the shearing flow theories of Benjamin (1959) and Miles (1962), this can be confirmed. For example, following Miles (1962), the parameter z, associated with transfer of energy through the viscous layer in the air to the water can be calculated. For a (measured) wave length $\bar{\lambda}$ = 10 cm and phase speed $\bar{c}_e$ = 40 cm/sec, U_∞ = 6 mps,

$$z \approx \frac{\bar{c}_e \bar{k}^{1/3} \nu_A^{1/3}}{U^{*4/3}} = 0.17 \quad ,$$

where $\bar{k}$ is the wave number corresponding to $\bar{\lambda}$. This value of z is quite typical of wind waves in the channel and is well within the range where positive transfer of energy to the water surface through the viscous layer is expected (See, for example, Miles (1962)).

Thus, in view of the previous remarks, it is useful to consider U^* as the important characteristic fluid velocity, rather than U_∞ or U_{avg}. In the following sections, the data for the water motion will be discussed in relation to the friction velocity based on the average shearing stress at the water surface as calculated from Fig. 6 and Eq. (3.2).

The Development of Waves and Currents. The growth with fetch of waves in the channel is reflected in two characteristic lengths, the standard deviation σ and the wave length $\bar{\lambda}$. The increase with F and U^* of σ and $\bar{\lambda}$ is shown in Fig. 9. The effect of depth is also shown in the drawing. Decrease in depth tends to reduce the wave length, and the standard deviation of the (larger) waves generated at higher wind speeds. Our data for σ, and $\bar{\lambda}$ were compared to those reported by Sibul (1955), whose results were given in terms of U_∞. For given values of U_∞ and d, the results of both these studies appeared to be essentially the same.

Two characteristic velocities are associated with the water motion. These are the surface velocity u_o, and the phase speed of significant waves, $\bar{c}_e$. The change with F, U^* and d of these properties is shown in Fig. 10. For a given wind speed, the surface drift tends to increase slightly with increasing fetch over the range of depth shown, except near the ends of the channel. The measured phase speed is approximately independent of depth down to 5.1 cm for U^* up to 0.63 mps. However, at higher values of U^*, the water depth begins to affect $\bar{c}_e$. The values of $\bar{c}_e$ generally increase with increasing friction velocity and fetch.

The ratio α ($= u_o/U_{avg}$) for data in the channel is the order of 0.017. An analysis in the Eulerian framework of the surface drift associated with growing laminar boundary layers for infinite depths of air and water indicates that α should be about 0.025 (Lock (1951)). The method of tracing buoyant particles on the water surface roughly measures paths of fluid particles, the fact the flow is steady in the mean implies that this technique also should indicate crudely the patterns of streamlines.

Thus, our experimental values of α are at least approximately comparable to Lock's predictions. It is interesting to note that the experiments and the (laminar) theory are remarkably close in agreement.

For a given ratio of air density to water density, Lock's analysis predicts that α should be a constant. The experimental results of this study and those of Keulegan (1951) and Masch (1963) indicate that α depends weakly on fetch, and more strongly on depth. Lock's analysis then should be considered a limiting theory. If this type of analysis were extended to include the possibility that the boundary layers in the air and the water begin to grow at different fetches, and that the water has finite depth, one might expect that α should depend on the Reynolds number, say Re_d ($= u_o d/\nu_w$), where ν_w is the kinematic viscosity of water.

Both Keulegan and Masch have found that their data for α can be correlated in terms of Re_d by the same curve. Several values of α were calculated from our data for F = 5 and 8 meters. Our results were taken at considerably higher altitude than Keulegan's so that the effect of altitude on the fluid density should be taken into account. Lock's theory suggests that α should be proportional to $\rho_A^{1/2}$. Using this relation, our data were corrected to correspond to sea level, and are shown with Keulegan's curve in Fig. 11. The theoretical value of α of Lock and Keulegan's asymptotic value of α also are indicated for comparison. In spite of the assumed correction for air density, our results are systematically lower by about 16% than the curve of Keulegan and Masch.

The Phase Speed and the Drift Current. The phase speed of significant waves as measured with respect to a fixed point ($\bar{c}_e$) was compared with values calculated from the theory for small amplitude gravity waves. The theoretical phase speed is:

$$\bar{c}_o = \left[(g\bar{k}^{-1}) \tanh(\bar{k}d) \right]^{1/2} \qquad (4.1)$$

where $\bar{k} = 2\pi/\bar{\lambda}$. In all cases, the values of $\bar{c}_e$ were larger than values calculated by Eq. (4.1). This effect has also been observed by Francis (1951) and Cox (1958). Francis qualitatively accounted for the deviation by considering an increase in wave velocity associated with the surface drift, and the fact that the waves are finite in amplitude. Cox, on the other hand,

attributed the difference to the combined effects of finite amplitude, orbital velocity of low-frequency wavelets, drift currents, and dynamic effects of the wind. Cox only analyzed in detail the finite amplitude effect as calculated by Sekerzh-Zenkovich (1956). Cox found that the influence of finite amplitude waves could only explain his observed increase in phase velocity for waves larger than $\bar{\lambda} \approx 7$ cm. The observed differences in phase speed for wavelets of length smaller than about 7 cm could not be accounted for by the effect of finite amplitude alone.

Although Cox mentioned that the drift current should be considered, he did not take this feature into account quantitatively in explaining differences between $\bar{c}_e$ and $\bar{c}_o$. For strict comparison to $\bar{c}_e$, $\bar{c}_o$ should be measured relative to an average transport in the water. Because the orbital movement of water particles associated with the waves extends downward to some depth, the surface drift u_o is not the proper correction factor. The correction should be proportional to a weighted average water velocity over some depth below the surface.

Lilly (1965) has proposed a drift correction for waves traveling on water at finite depth. Assuming that the vertical profile of the drift current is parabolic (laminar flow), and that the waves have infinitesimal amplitudes, Lilly found that

$$\bar{c}_T = \bar{c}_o \left\{ 1 + \frac{u_o}{c_o} \left[1 + \frac{3}{2(\bar{k}d)^2} - \frac{1 + 2\cosh(2\bar{k}d)}{(\bar{k}d)\sinh(2\bar{k}d)} \right] \right\} \quad (4.2)$$

For deep water, $kd \to \infty$ and Eq. (4.2) implies that the waves travel with the surface flow only (i.e., $\bar{c}_T \approx c_o + u_o$). However, for shallow water, $kd \to 0$, and Eq. (4.2) predicts, as expected, that $\bar{c}_T \to \bar{c}_o$.

The values of $\bar{c}_T$ as calculated by Eq. (4.2) were compared to the corresponding experimental data, and the results are shown in Fig. 12. Experiment and theory agree within $\pm$ 15%. This error is approximately that expected on the basis of experimental errors in estimation of $\bar{c}_e$, and $\bar{c}_T$ using $\bar{\lambda}$ and u_o.

Systematic deviations between $\bar{c}_e$ and $\bar{c}_T$ might be expected since both the effect of surface tension and of finite wave amplitude were not considered in deriving Eq. (4.2). The correction in $\bar{c}_T$ for surface tension in deep water waves was found to be negligible for the experimental observations. However, the Stokes correction of $\bar{c}_T$ for gravity waves of

finite amplitude (e.g., Lamb (1932)) could vary from 1% to 11% (increase) if it is assumed that the amplitude of significant waves is 3.0σ (e.g., Sibul (1955)). Thus, Lilly's equation would give values of $\bar{c}_T$ somewhat larger on the average than the experimental data.

The effect of finite amplitudes in the wind waves may be offset partially by the influence of turbulence in the water. Dye traces of the motion in the water indicate that the water flow was turbulent and not laminar. The use of a turbulent velocity profile having a steeper gradient near the surface than the parabolic curve but having the same drift velocity at the surface would result in a smaller correction factor for drift than predicted by Eq. (4.2).

These results indicate, as might be expected, that the significant wind waves on the water in the channel travel relative to a mean drift essentially as gravity waves of small amplitude.

5. WAVE SPECTRA

Autocorrelation Functions and the Frequency Spectra. The time correlations between displacements of the water surface were calculated from the digitized depth gauge data. The autocorrelation function $R(\tau)$ is defined as:

$$R(\tau) = \frac{}{\xi(t_1)\ \xi(t_2)} \quad , \qquad \tau = t_2 - t_1 \tag{5.1}$$

where $\xi(t_1)$ and $\xi(t_2)$ are surface displacements taken at the same point for two different times, t_1 and t_2. The averaging technique in Eq. (5.1) was carried out after the method given in Blackman and Tukey (1958).

The function $R(\tau)$ for waves in the channel was found to exhibit certain interesting features. A typical example is shown in Fig. 13. $R(\tau)$ was generally found to oscillate regularly about the $R(\tau) = 0$ line with increasing τ. Its amplitude decreased sharply initially, but it became fairly steady at higher values of τ, though sometimes it varied slowly as if a lower harmonic was present. The behavior of $R(\tau)$ is consistent with the visual observation that there is a tendency for the mutual action of the two fluids to force a nearly periodic, regular disturbance to develop on the water at a given fetch in the channel. On the regular waves are superimposed small, random disturbances which are related to the larger values of $R(\tau)$ for small τ.

It is well known that the autocorrelation of a periodic function of period P is another periodic function with period P and a zero mean. Hence, the period of the significant waves can be estimated from the zero crossings of the autocorrelation function at large values of τ where the effects of the random component are small. As seen in Fig. 13, the components of "noise" tend to damp out rapidly, so that the period of the significant waves also can be calculated approximately from zero crossings of $R(\tau)$ over the whole range of τ. Typical values of 1/? found in this manner are listed in Table I.

The energy spectra were calculated by means of the following relation:

$$\Phi(f) = \int_0^\infty R(\tau) \cos 2\pi f \tau d\tau. \qquad (5.2)$$

The scheme for evaluating the integral in Eq. (5.2) for a finite record is given by Blackman and Tukey (1958). However, instead of the usual technique of "hanning", it was preferred to obtain a suitable lag window by multiplying the function $R(\tau)$ by:

$$g(\tau) = \left(1 + \cos\frac{\pi \tau}{T_m}\right) , \qquad (5.3)$$

where T_m for our data is 3.5. the fading function $g(\tau)$ has the advantage of suppressing the periodic component in the autocorrelation function at large lags without removing any information at short lags. An example of the faded autocorrelation $R'(\tau)$ (=Rg) corresponding to the curve of $R(\tau)$ is shown in Fig. 13.

The spectrum corresponding to the faded autocorrelation $R'(\tau)$ in Fig. 13 is shown in Fig. 14. Note that the tendency towards periodicity in the wave train also is indicated in this spectrum. Higher harmonics of the frequency f_m for which the energy is maximum appear as indicated in this drawing. If the waves were perfectly periodic, the idealized spectrum based on the $R(\tau)$ curve would develop as spikes of infinite height at n multiples of f_m. However, because the waves are not truly periodic, and because of the random components which exist in the signal, the spectrum actually takes the bumpy shape indicated in Fig. 14.

Assuming that the frequency where the maximum in the spectrum occurs is related to the properties significant waves, f_m ($\approx 1/P$) can be

compared to $\bar{c}_e/\bar{\lambda}$. Typical examples of f_m, 1/P and $\bar{c}_e/\bar{\lambda}$ are shown in Table I. Because of the narrowness of the region containing most of the energy in the spectra for wind generated waves in the channel, these three estimates of the frequency f_m are approximately equal. Thus, for practical purposes, the waves in the channel may be characterized essentially by the properties associated with the significant waves.

The Growth of Waves in the Channel. The frequency spectra calculated at different fetches for the same air velocity indicate how the waves grow as they move downstream along the channel. A typical set of spectra for increasing fetch is shown in Fig. 15A. The estimates of spectral density here are denoted by $\bar{\Phi}$. These values have been corrected by subtracting out the noise level, and have been smoothed by a method similar to that discussed by Hidy and Plate (1965). Near the leading edge of the water (small fetch), the observed spectrum contains little total energy and is rather broad. As the waves travel downstream, the magnitude of the spectral density function increases, the primary peaks tend to sharpen up while the values of f_m decrease.

The growth of waves in the range of higher frequencies tends to be limited as indicated in Fig. 15A. The complete mechanism for restraining the growth of the high frequency components is not known. However, it can be seen that the limitation in growth, in part, can be the result of attaining a balance between gains in energy input from the air and losses by dissipation. The dissipation of energy in small gravity-capillary waves is probably related to the action of viscosity, and surface tension. The loss by viscous forces in waves is proportional to $(ak)^2$ (Lamb (1932)) where a is the amplitude of a wave. As proposed by Longuet-Higgins (1962), the loss resulting from the indirect effects of surface tension can be related to the drain of energy from larger waves when capillary ripples are formed near the crests of the larger components. This particular mechanism indicates that the energy loss is proportional to $(a_c^2 k_c^3)$. The subscript c refers to the capillary ripple on the crest of a larger wave. If the interaction between components in the wave train is a second or higher order effect (e.g., Phillips (1963)), the action of dissipative processes should balance the input of energy from the air motion in such a way that the net energy at equlibrium is smaller the higher the frequency range. This is suggested in the behavior of the spectra shown in Fig. 15A.

It is interesting to note that the growth of components in the lower frequency range, say $f \leq 3.5$ cps in Fig. 15A is approximately exponential with fetch. This is illustrated in Fig. 15B. Here the logarithm of the spectral density for the component of the spectrum corresponding to f_m at F = 10.6 meters is plotted with fetch. Up to $F \approx 7$ meters, the growth of this component is essentially exponential. For $F > 7$ meters, the effects of dissipation begin to counteract the energy input and cause this component to tend to reach an equilibrium value of $\bar{\Phi}$.

Qualitatively the exponential growth observed with fetch has been predicted by the recent instability theories such as those of Miles (See, for example, Miles (1960)). This particular aspect of wave development in the channel will be discussed in more detail in another paper.

Similarity Shape of the Spectrum. An important feature which was also exhibited by many of the spectra for the channel waves was the tendency for growth in such a way that a similarity shape in the spectral density function is maintained. The frequency spectrum can be expressed, with Eq. (5.2) in normalized form, as:

$$\frac{\bar{\Phi} f_m}{\sigma^2} = \Psi(f/f_m) \qquad (5.4)$$

where Ψ denotes a dimensionless quantity representing a "universal" spectral density function.

Typical spectra which have been smoothed and corrected for noise level after Hidy and Plate (1965) are plotted in a form corresponding to Eq. (5.4) in Fig. 16. The spectra in Fig. 16 serve to define the similarity function Ψ quite well. The conditions of U^*, F and d for these spectra are shown in Table II along with the values of σ, f_m and Φ_m. In general, it was found that the channel data followed quite satisfactorily for the range $0.34 < U^* < 1.3$, and for $3 < F < 12$ meters.

Phillips (1958a) has shown on dimensional grounds that the equilibrium or saturation region in the high frequency region of the spectra for gravity waves should follow the f^{-5} rule. In contrast, it has been suggested by Hicks (See, for example, Phillips (1958b)) that the pure capillary spectrum should follow an $f^{-7/3}$ rule. As indicated in Fig. 16 the dimensionless spectra for waves in the channel tend to follow the f^{-5} rule over approximately two decades in the high frequency range. In the highest

frequency ratios, there is a tendency for some of the spectra to develop a slope less than -5. Capillary wave behavior should begin to appear above $f \approx 13$ cps in the frequency spectra. Only two cases, 163 and 188 shown in Fig. 16 actually reach this range. For case 163, capillary waves should appear for $f/f_m = 2.7$ to 3.0, while, for case 188, $f/f_m = 6.8$ to 7.0. Thus, in Fig. 16, these two examples may display the beginnings of a transition to the $f^{-7/3}$ range.

It should be noted, of course, that if the $f^{-7/3}$ range exists the similarity shape Ψ will not be preserved at high values of f/f_m. A tendency for the curves for cases 163 and 188 to break away from the average curve at different values of f/f_m can be seen in Fig. 16.

Unfortunately, the existence of the $f^{-m/3}$ rule cannot be verified generally in these results because the highest frequencies which can be resolved with some accuracy in the computation scheme used lies around 15 cps. Therefore, these data cannot provide conclusive evidence for the existence of an equilibrium range in capillary waves.

ACKNOWLEDGEMENT

The wind-water tunnel at Colorado State University was constructed under a matching grant from the National Science Foundation. This work was supported by the National Science Foundation in connection with its grant to Colorado State University, and its contract with the National Center for Atmospheric Research. The authors are grateful to R. Bird, C. Goodwin, Hosein Shokouh, C. Yang and many others for their efforts in carrying out the experimental program and analyzing the extensive data of this study. The authors also appreciate very much the helpful comments of Prof. O. M. Phillips.

REFERENCES

BAINES, W. D., and D. J. KNAPP 1965 Proc. A.S.C.E. (Journal Hydraulics Division) 91, 205.

BENJAMIN, T. B. 1959 J. Fluid Mech. 6, 161.

BLACKMAN, R. B., and J. W. TUKEY 1958 The Measurement of Power Spectra. New York: Dover.

COHEN, L. S., and T. S. HANRATTY 1965 A. I. Ch. E. Journal 11, 138

COX, CHARLES 1958 J. Mar. Res. 16, 199.

FITZGERALD, L. M. 1963 Aust. J. Phys. 16, 475.

FRANCIS, J. R. D. 1951 Proc. Roy. Soc. (London) A 206, 387.

GOODWIN, C. R. 1965 "The Effect of Wind Drag on Open-channel Flow," unpublished M.S. thesis, Colorado State University, Ft. Collins Colorado.

HICKS, B. L. 1963 Ocean Wave Spectra. Englewood Cliffs, N. J.: Prentice-Hall, Inc.

HIDY, G. M., and E. J. PLATE 1965 On the Frequency Spectrum of Wind Generated Waves, to be published in Phys. of Fluids.

HOLMES, P. 1963 "Wind Generation of Waves," unpublished Ph.D. Dissertation, University College of Swansea.

KEULEGAN, G. H. 1951 Res. Nat. Bur. Stand. 46, 358.

KUNISHI, H. 1963 Bull. Disaster Prev. Res. Inst. No. 61, Disaster Prev. Res. Inst., Kyoto, Japan.

LAMB, H. 1932 Hydrodynamics. New York: Dover.

LILLY, D. K. 1965 On the Speed of Surface Gravity Waves Propogating in a Moving Fluid. Submitted to J. Fluid Mech.

LOCK, R. C. 1951 Quart. J. Mech. & Applied Math. 4, 42.

LONGUET-HIGGINS, M. S. 1962 J. Fluid Mech. 16, 138.

MASCH, F. 1963 Int. J. Water & Air Poll. 7, 697.

MILES, J. W. 1960 J. Fluid Mech. 7, 469.

MILES, J. W. 1962 J. Fluid Mech. 13, 433.

PHILLIPS, O. M. 1958a J. Fluid Mech. 4, 426.

PHILLIPS, O. M. 1958b J. Mar. Res. 16, 226.

PHILLIPS, O. M. 1963 Ocean Wave Spectra. Englewood Cliffs, N. J.: Prentice-Hall, Inc.

SCHLICHTING, H. 1960 Boundary Layer Theory. 4th Ed., New York: McGraw Hill.

SCHOOLEY, A. H. 1963 J. Geophys. Res. 68, 5497.

SEKERZH-ZENKOVICH, Y. I. 1956 Dokl. Akad. Nauk. S.S.S.R. 109, 913.

SIBUL, O. 1955 U. S. Army Corps of Engineers, Beach Erosion Board, Tech. Memo, No. 72.

TOWNSEND, A. A. 1956 The Structure of Turbulent Shear Flow, Cambridge University Press.

TUCKER, M. M., and H. CHARNOCK 1955 "A Capacitance-wire Recorder for Small Waves," in Proc. of the 5th Conference on Coastal Engineering, Council of Wave Research, University of California, Berkeley.

WIEGEL, R. L. 1961 Proc. 7th Conf. on Coastal Eng., Council of Wave Research, Eng. Foundation, Berkeley, California.

WIEGEL, R. L. 1963 Ocean Wave Spectra. Englewood Cliffs, N. J.: Prentice-Hall, Inc.

URSELL, F. 1956 Surveys in Mechanics. Cambridge University Press.

LIST OF CAPTIONS

Table I. Comparison between frequency of significant waves in cps as estimated from the ratio $\bar{c}_e/\bar{\lambda}$, from $R(\tau)$, and from $\Phi(f)$.

Table II. Typical properties of waves generated by air blowing over water standing in a channel.

Fig. 1. A schematic drawing of air and water motion associated with growing waves on a water surface.

Fig. 2. A general view of the wind-water tunnel.

Fig. 3. Variation in the pressure gradient in air with air speed in the wind-water tunnel. The pressure gradient is given in terms of length of water per length of channel.

Fig. 4. Typical distributions of air flow in the wind-water tunnel.
A. Vertical profiles taken along the center section, and
B. Horizontal profiles taken at $(z - d) \approx 20$ cm.

Fig. 5. Distribution of air velocity at a given cross-section, in the channel.

Fig. 6. The variation of average shearing stress coefficient with mean air velocity.

Fig. 7. A typical example of the properties of the air boundary layer growing over water in the channel.

Fig. 8. A similarity distribution for the air velocities along the center section of the tunnel.

Fig. 9. Variation in characteristic lengths of surface waves with mean friction velocity, fetch, and water depth.

Fig. 10. Variation in characteristic water velocities with mean friction velocity, fetch, and depth.

Fig. 11. Correlation of surface drift with Reynolds number, Re_d, after Keulegan (1951).

Fig. 12. Comparison between experimental values of the phase speed of significant waves and values calculated by Lilly's theory.

Fig. 13. Typical unfaded and faded autocorrelation functions for the displacement of the water surface.

Fig. 14. The energy spectrum corresponding to the faded autocorrelation in Fig. 13.

Fig. 15. A. Growth of waves with fetch in the channel as indicated by the changes in frequency spectra.

B. The exponential growth of a low frequency component of the wave spectrum.

Fig. 16. The similarity spectrum for wind generated waves in the channel. After Hidy and Plate (1965).

Plate I. The development of wind waves on water 10.7 cm deep at a fetch of 8 meters along the channel.

A. U_∞ = 4 mps, $\bar{\lambda} \approx 3$ cm;

B. U_∞ = 6.1 mps, $\bar{\lambda} \approx 12$ cm;

C. U_∞ = 7.6 mps, $\bar{\lambda} \approx 15$ cm;

D. U_∞ = 9.8 mps, $\bar{\lambda} \approx 24$ cm.

TABLE I.

Case	$\bar{c}_e/\bar{\lambda}$	1/P	f_m
21	2.74	2.87	2.91
79	4.62	4.83	4.74
100	5.61	5.71	5.65
113	2.91	2.85	2.76
169	3.24	3.31	3.26

TABLE II.

Case	d(meters)	U_∞(mps)	U*(mps)	F(meters)
163	0.0254	6.10	0.27	5.24
175	0.102	10.7	0.61	10.7
188	0.102	17.4	1.1	8.16
192	0.0508	10.7	0.61	11.5
208	0.0508	9.15	0.50	7.86
212	0.102	10.7	0.61	5.74

Case	$\sigma \times 10^2$ (meters)	f_m(cps)	Φ_m(m^2-sec)
163	0.131	4.83	2.90×10^{-4}
175	0.767	2.36	7.99×10^{-3}
188	1.36	1.93	2.97×10^{-2}
192	0.538	2.33	5.53×10^{-3}
208	0.614	2.48	8.65×10^{-3}
212	0.457	3.17	4.15×10^{-3}

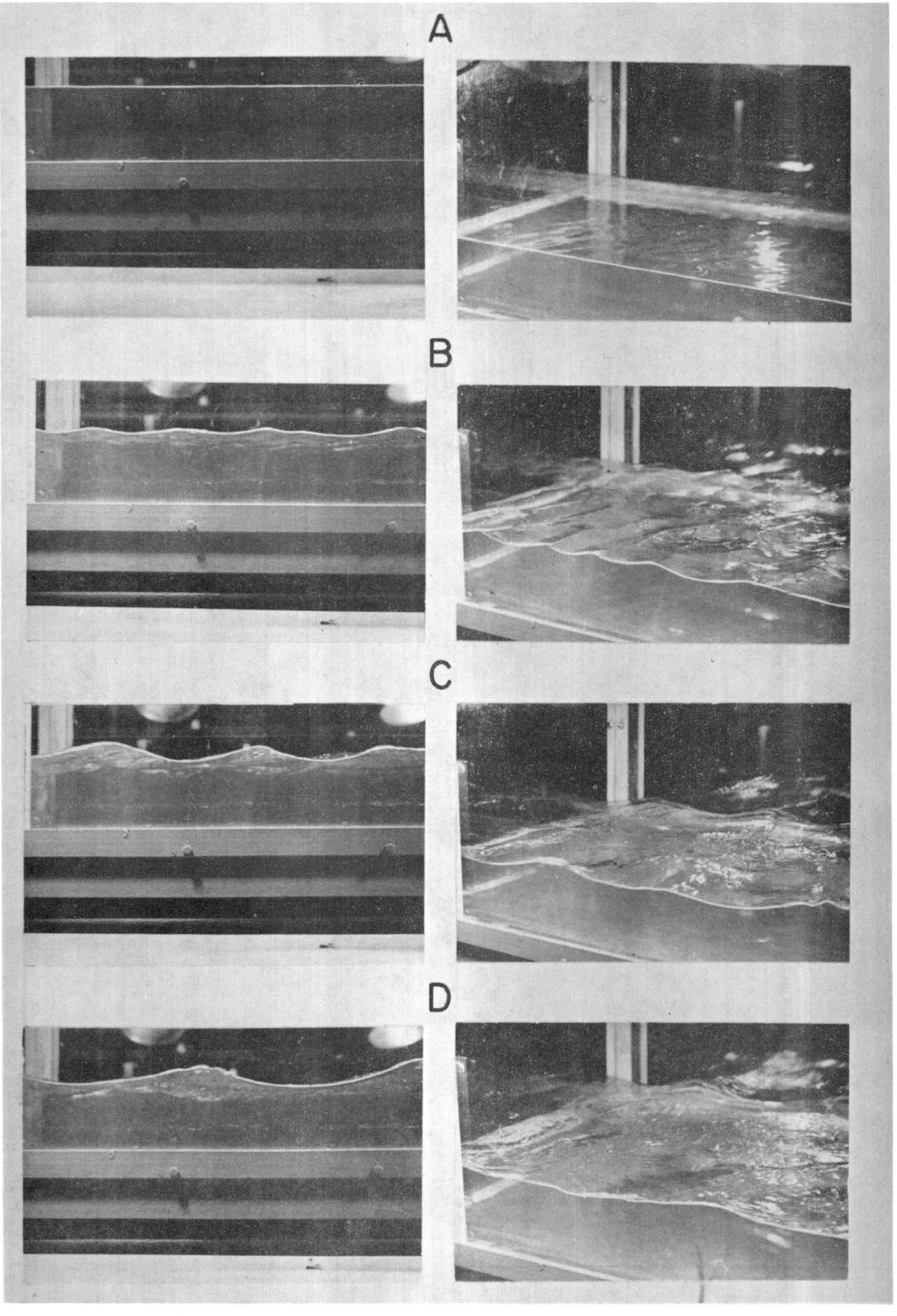
A
B
C
D

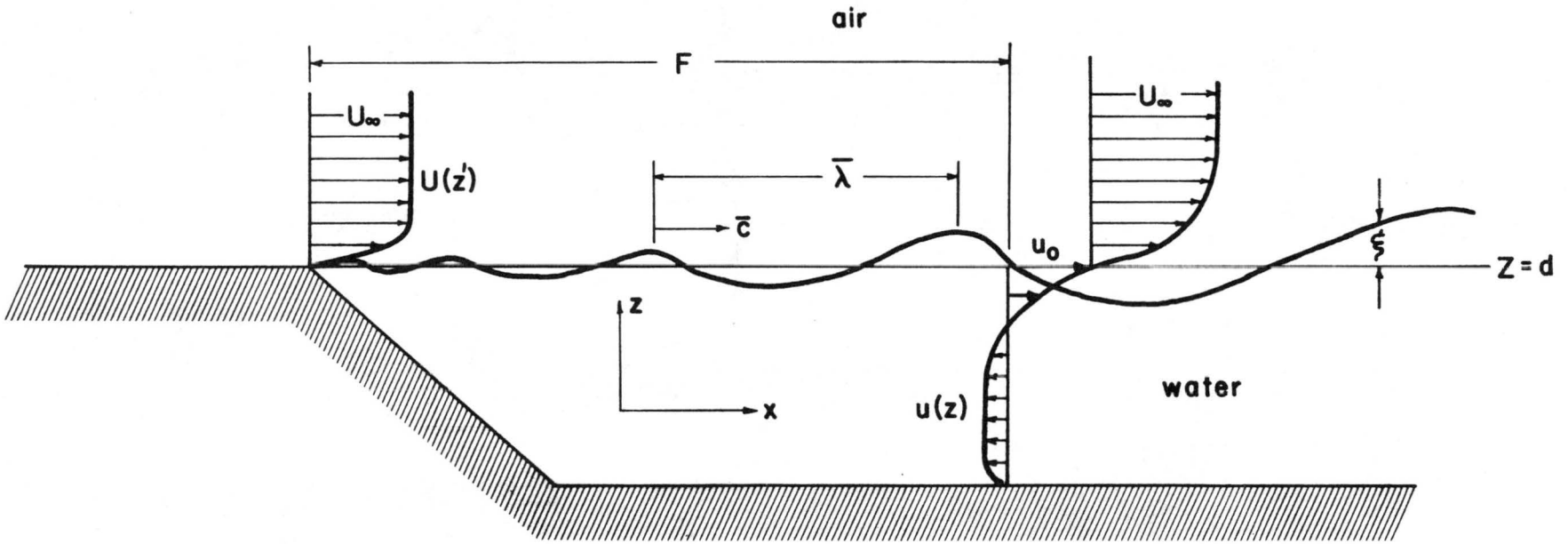

Figure 1

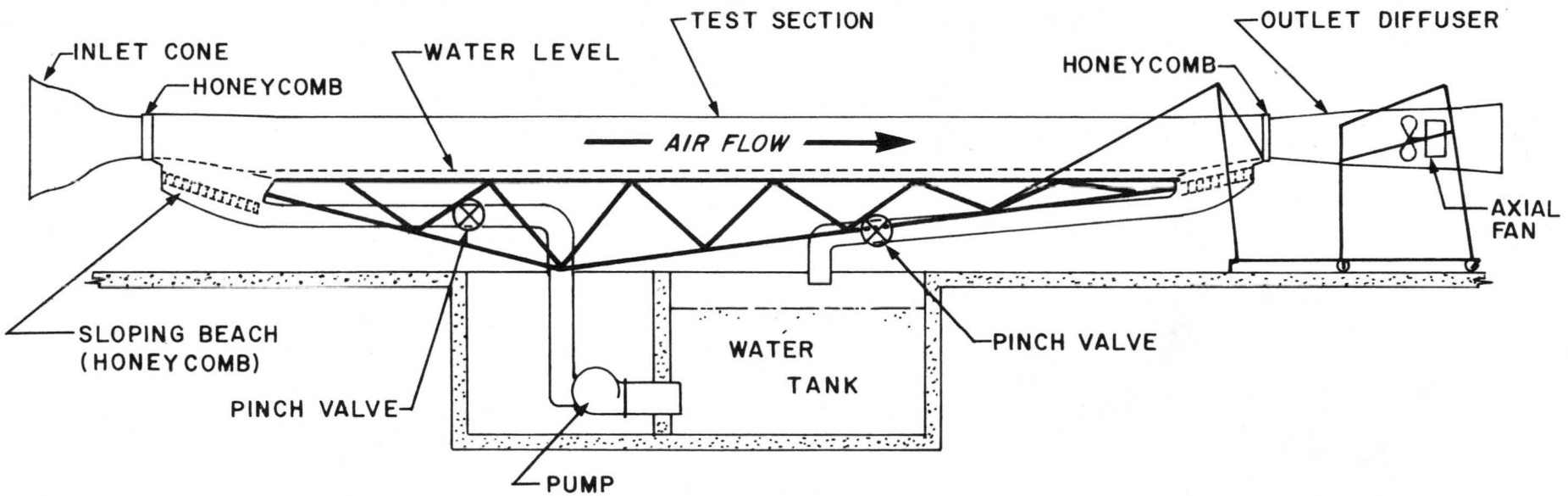
INLET CONE
HONEYCOMB
WATER LEVEL
TEST SECTION
AIR FLOW
HONEYCOMB
OUTLET DIFFUSER
AXIAL FAN
SLOPING BEACH (HONEYCOMB)
PINCH VALVE
WATER TANK
PINCH VALVE
PUMP

Figure 2

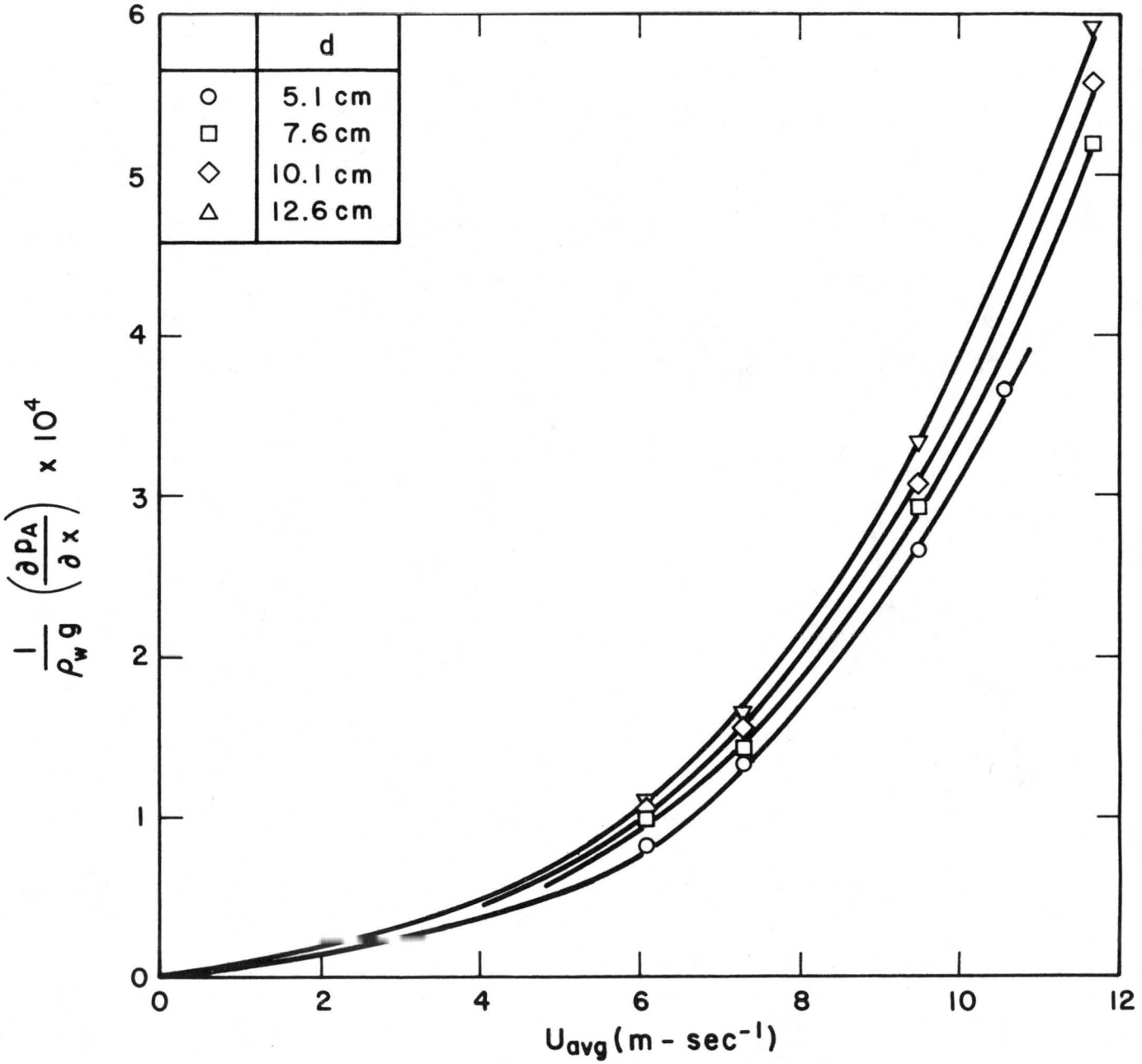
d
5.1 cm
7.6 cm
10.1 cm
12.6 cm
$\frac{1}{\rho_w g}\left(\frac{\partial p_A}{\partial x}\right) \times 10^4$
U_{avg} (m - sec^{-1})
0
1
2
3
4
5
6
0
2
4
6
8
10
12

Figure 3

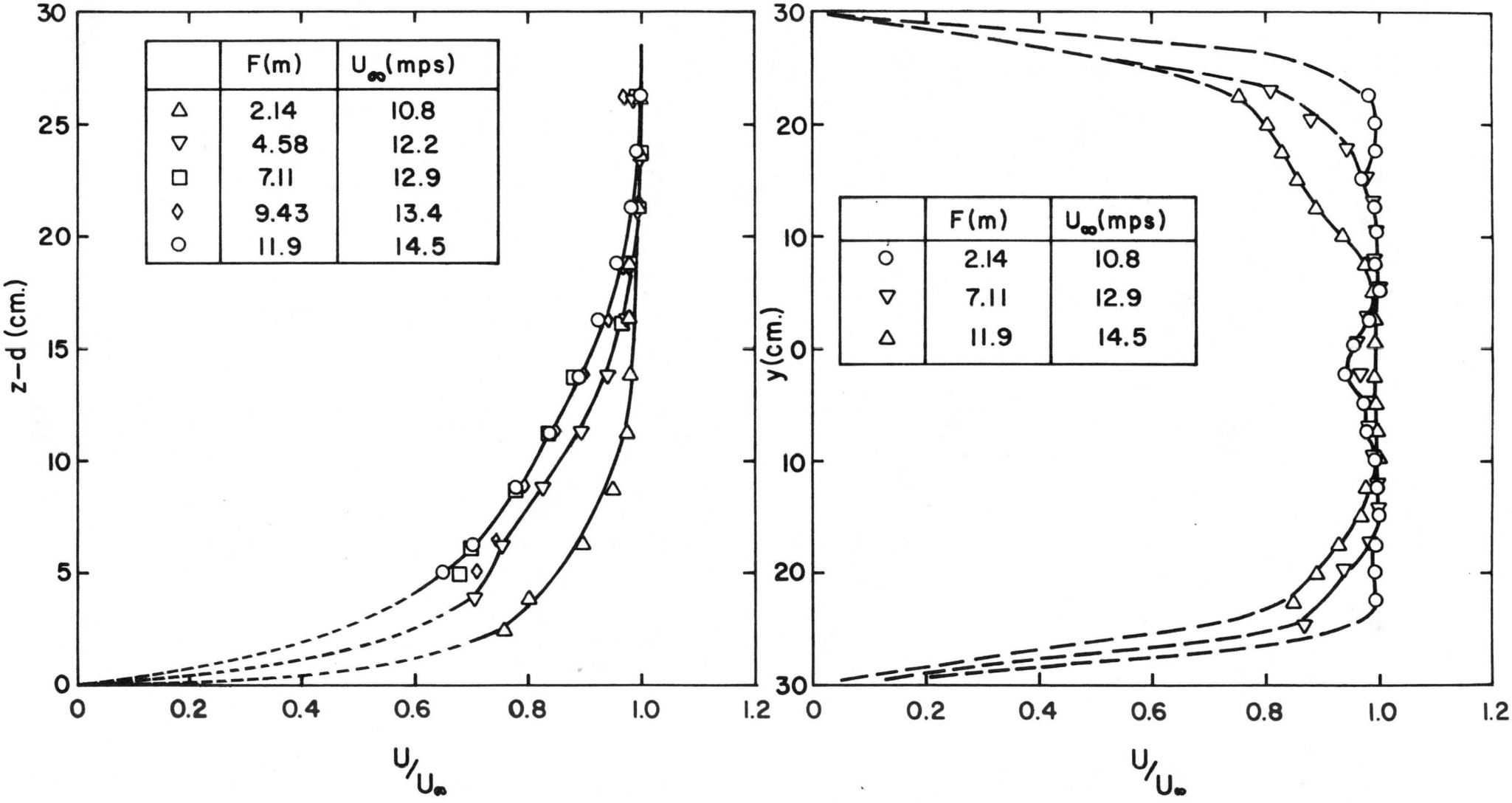
F(m)
U_∞(mps)
2.14
10.8
4.58
12.2
7.11
12.9
9.43
13.4
11.9
14.5
z-d (cm.)
U/U_∞
F(m)
U_∞(mps)
2.14
10.8
7.11
12.9
11.9
14.5
y(cm.)
U/U_∞

Figure 4

A

B

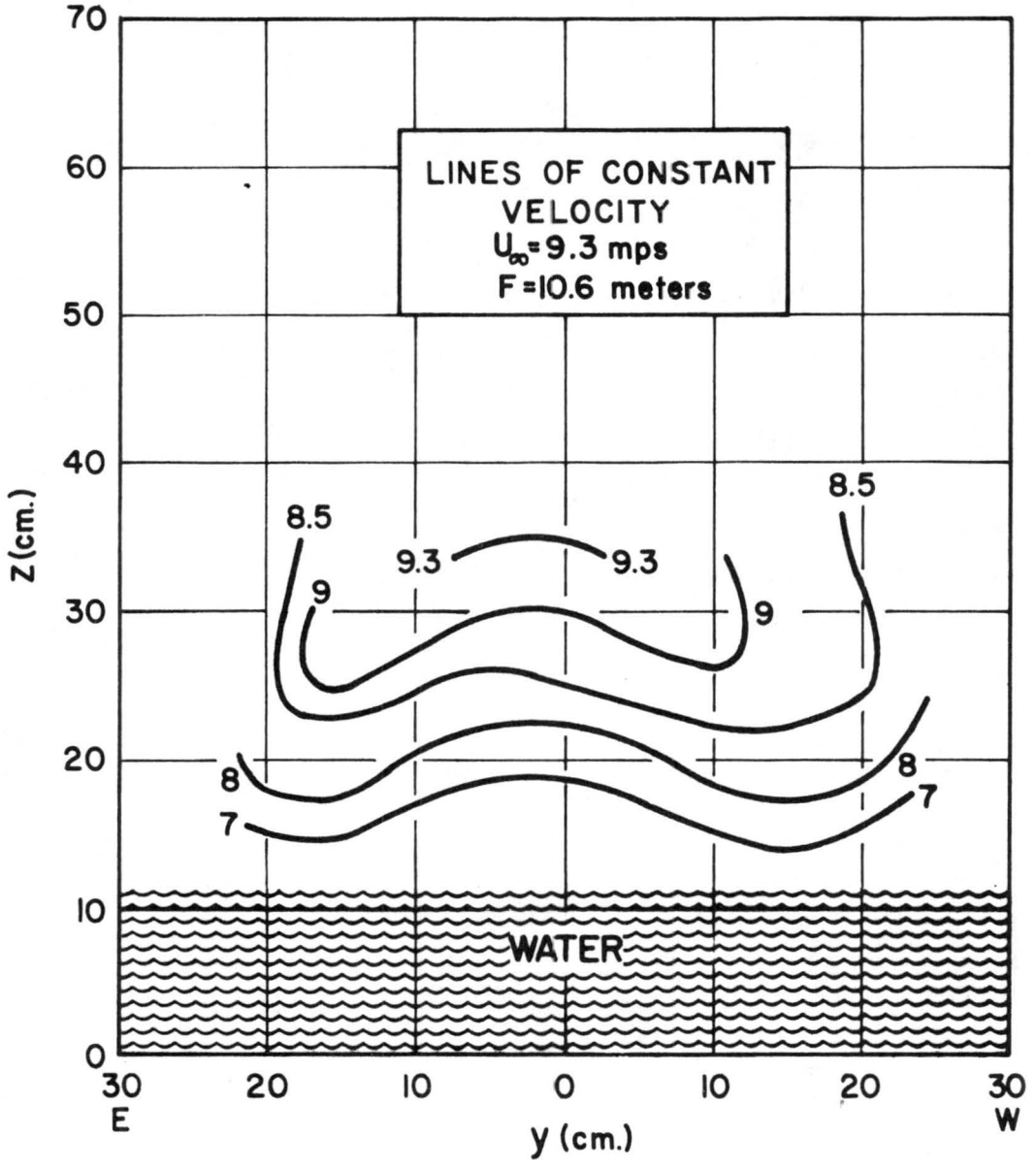
LINES OF CONSTANT
VELOCITY
U_∞ = 9.3 mps
F = 10.6 meters
Z (cm.)
y (cm.)
WATER
8.5
9.3
9
8
7
70
60
50
40
30
20
10
0
30
20
10
0
10
20
30
E
W

Figure 5

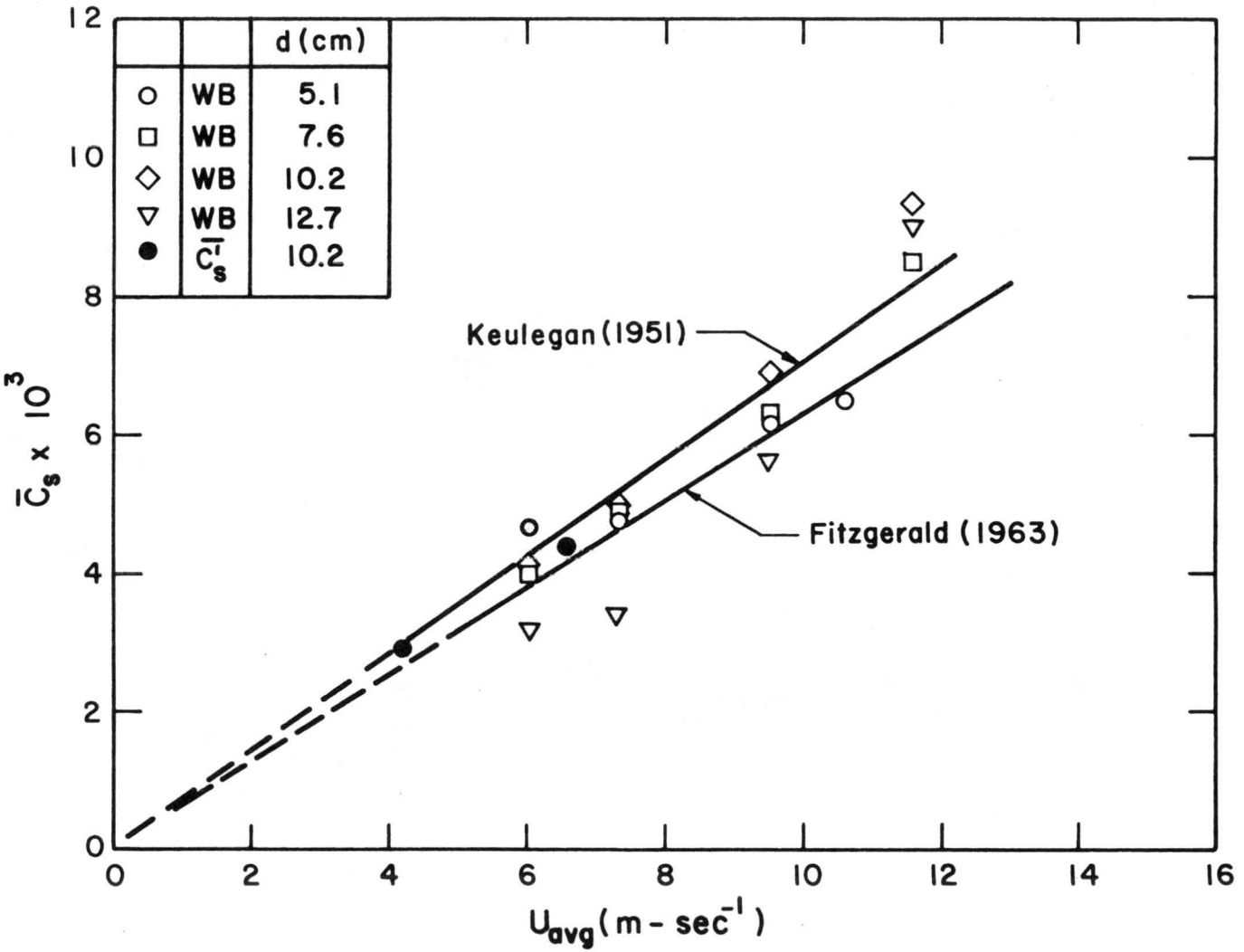
d (cm)
WB 5.1
WB 7.6
WB 10.2
WB 12.7
$\bar{C}'_s$ 10.2
Keulegan (1951)
Fitzgerald (1963)
$C_s \times 10^3$
U_{avg} (m - sec^{-1})
0
2
4
6
8
10
12
14
16

Figure 6

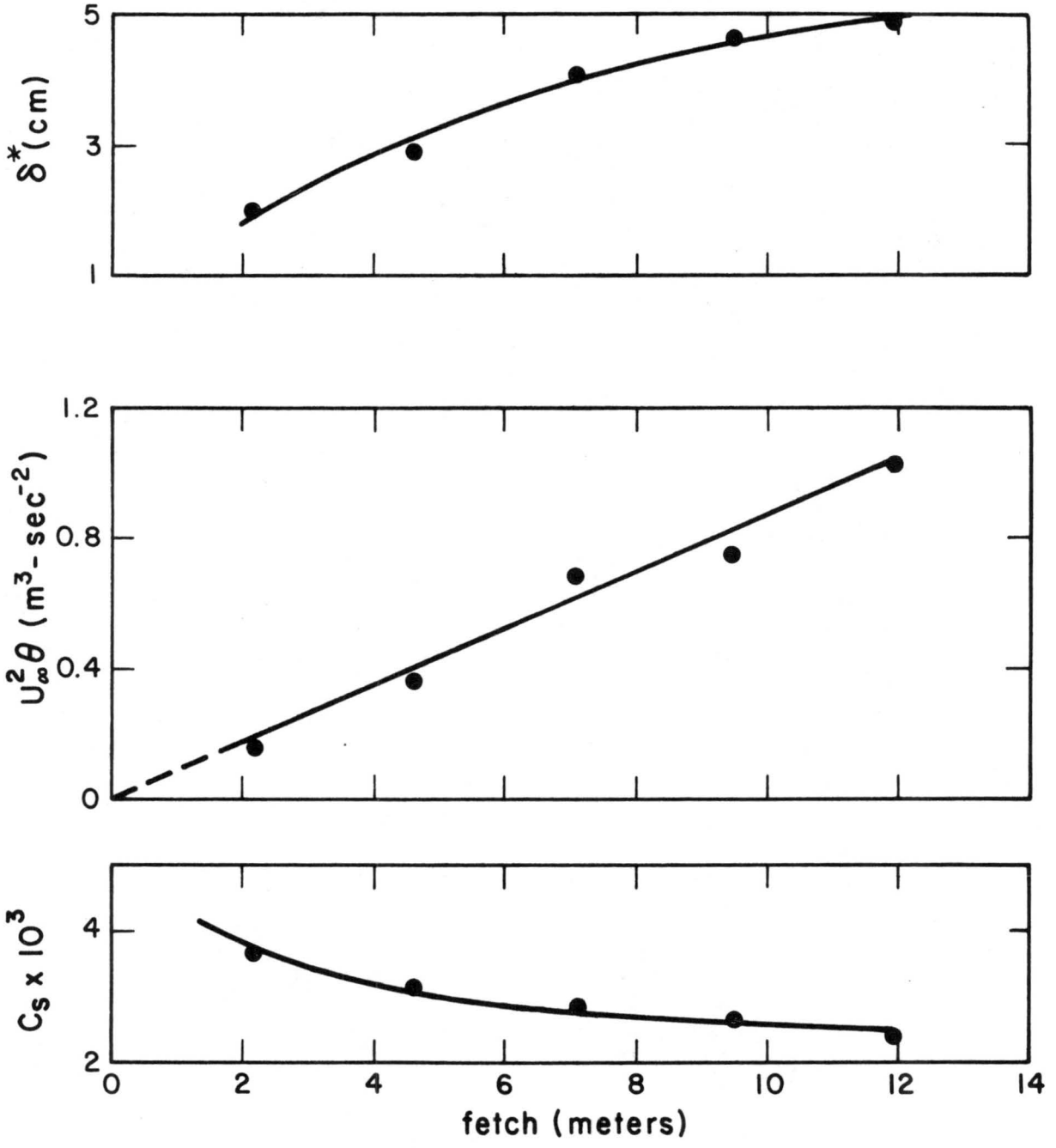
5
3
1
δ*(cm)
1.2
0.8
0.4
0
$U_\infty^2\theta$ (m^3-sec^{-2})
4
2
$C_S \times 10^3$
0
2
4
6
8
10
12
14
fetch (meters)

Figure 7

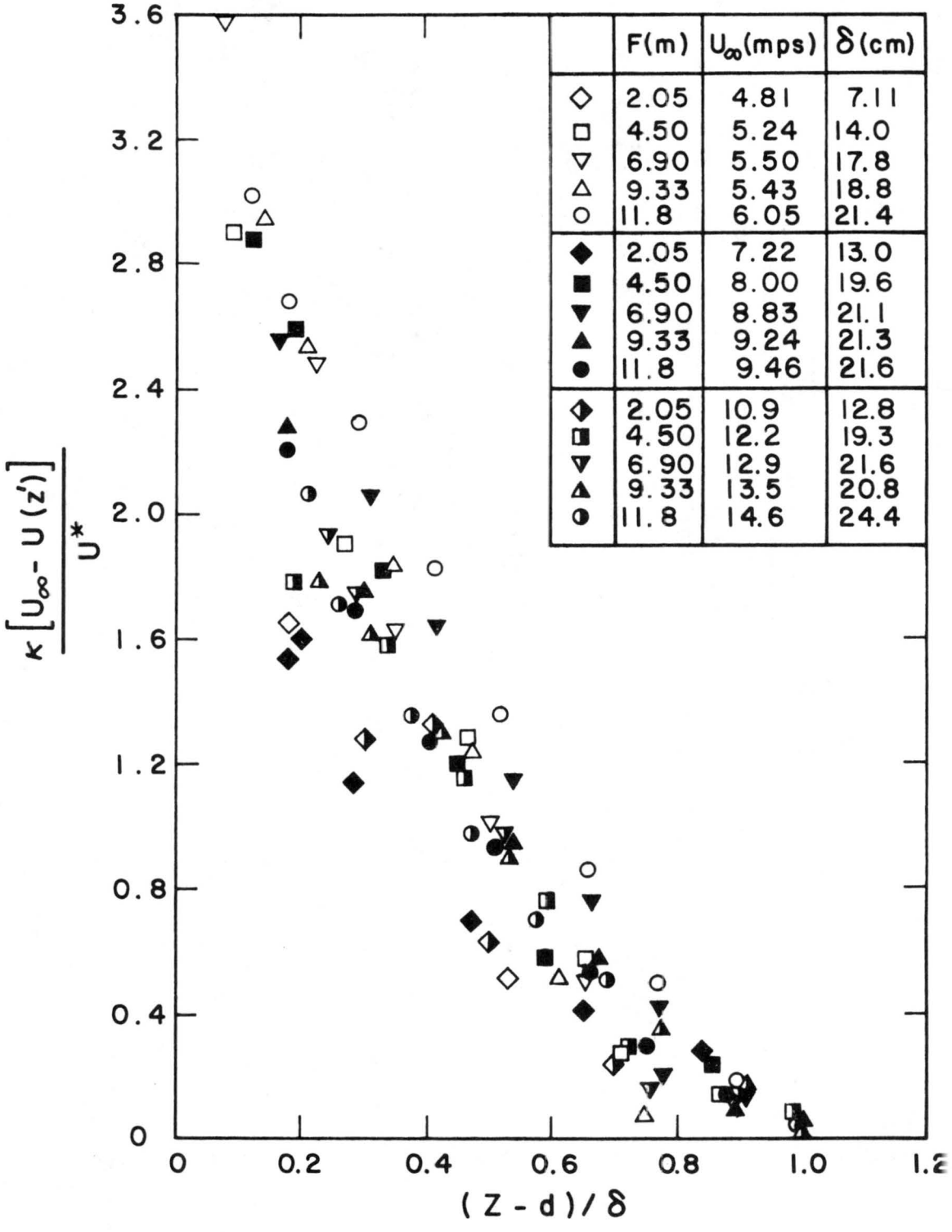
F(m) | U_∞(mps) | δ(cm)
2.05 | 4.81 | 7.11
4.50 | 5.24 | 14.0
6.90 | 5.50 | 17.8
9.33 | 5.43 | 18.8
11.8 | 6.05 | 21.4
2.05 | 7.22 | 13.0
4.50 | 8.00 | 19.6
6.90 | 8.83 | 21.1
9.33 | 9.24 | 21.3
11.8 | 9.46 | 21.6
2.05 | 10.9 | 12.8
4.50 | 12.2 | 19.3
6.90 | 12.9 | 21.6
9.33 | 13.5 | 20.8
11.8 | 14.6 | 24.4
$\frac{\kappa[U_\infty - U(z')]}{U^*}$
(Z - d)/δ
0
0.2
0.4
0.6
0.8
1.0
0.4
0.8
1.2
1.6
2.0
2.4
2.8
3.2
3.6

Figure 8

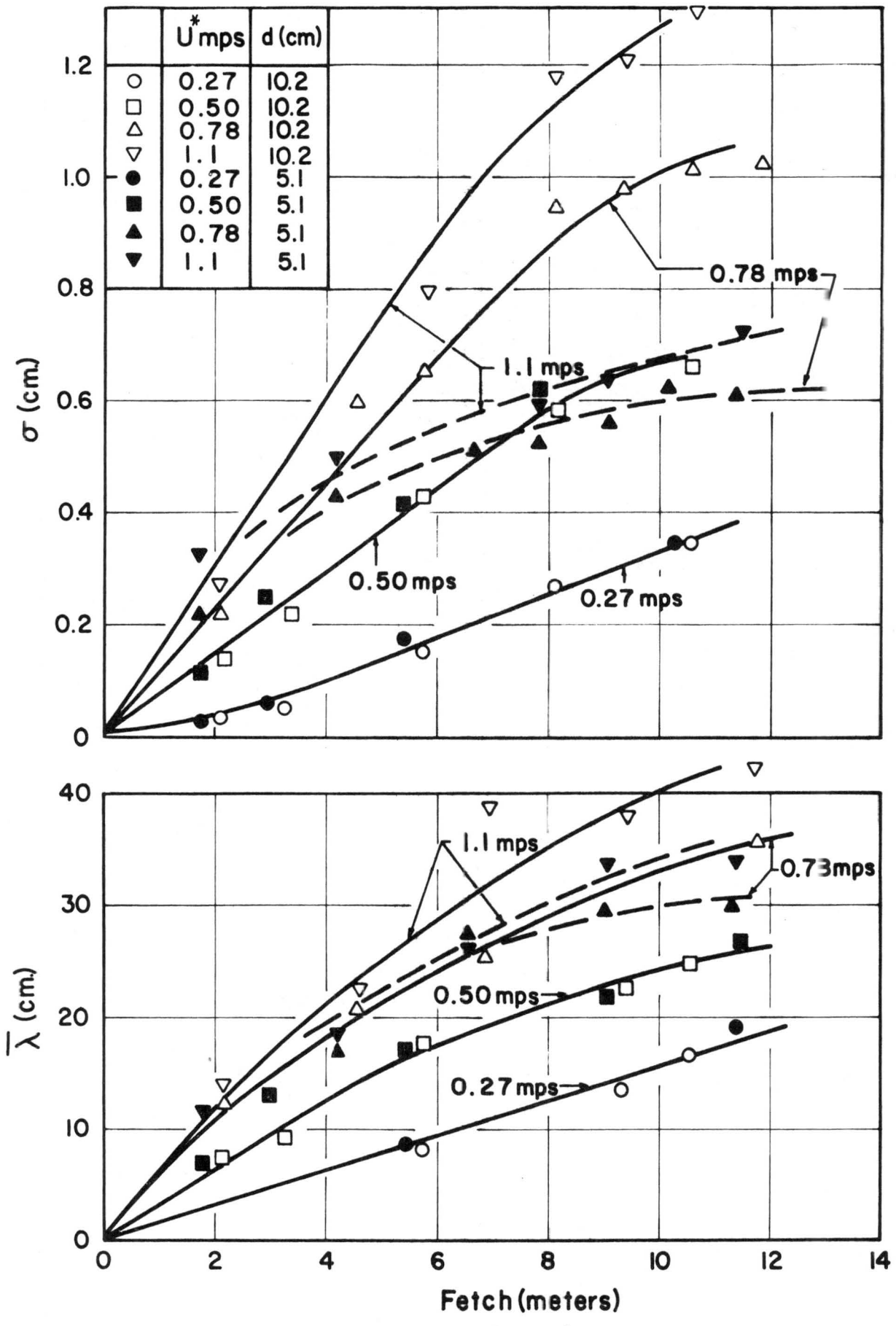
U* mps
d (cm)
0.27 10.2
0.50 10.2
0.78 10.2
1.1 10.2
0.27 5.1
0.50 5.1
0.78 5.1
1.1 5.1
σ (cm.)
0.78 mps
1.1 mps
0.50 mps
0.27 mps
λ̄ (cm.)
1.1 mps
0.73mps
0.50 mps
0.27 mps
Fetch (meters)

Figure 9

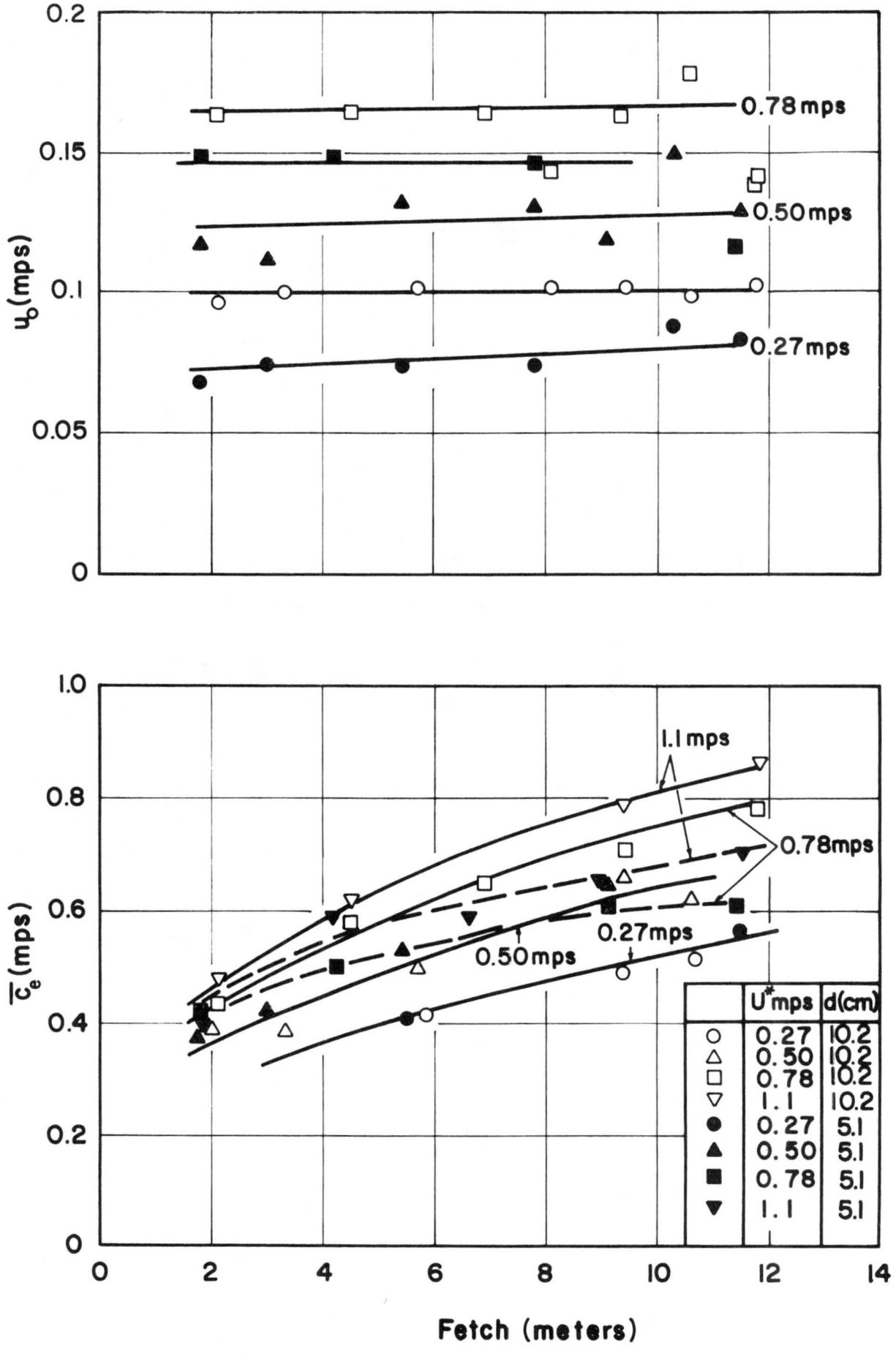
0.2
0.15
0.1
0.05
0
u_0(mps)
0.78mps
0.50mps
0.27mps
1.0
0.8
0.6
0.4
0.2
0
$\overline{c}_e$(mps)
1.1mps
0.78mps
0.27mps
0.50mps
U*mps
d(cm)
0.27 10.2
0.50 10.2
0.78 10.2
1.1 10.2
0.27 5.1
0.50 5.1
0.78 5.1
1.1 5.1
0
2
4
6
8
10
12
14
Fetch (meters)

Figure 10

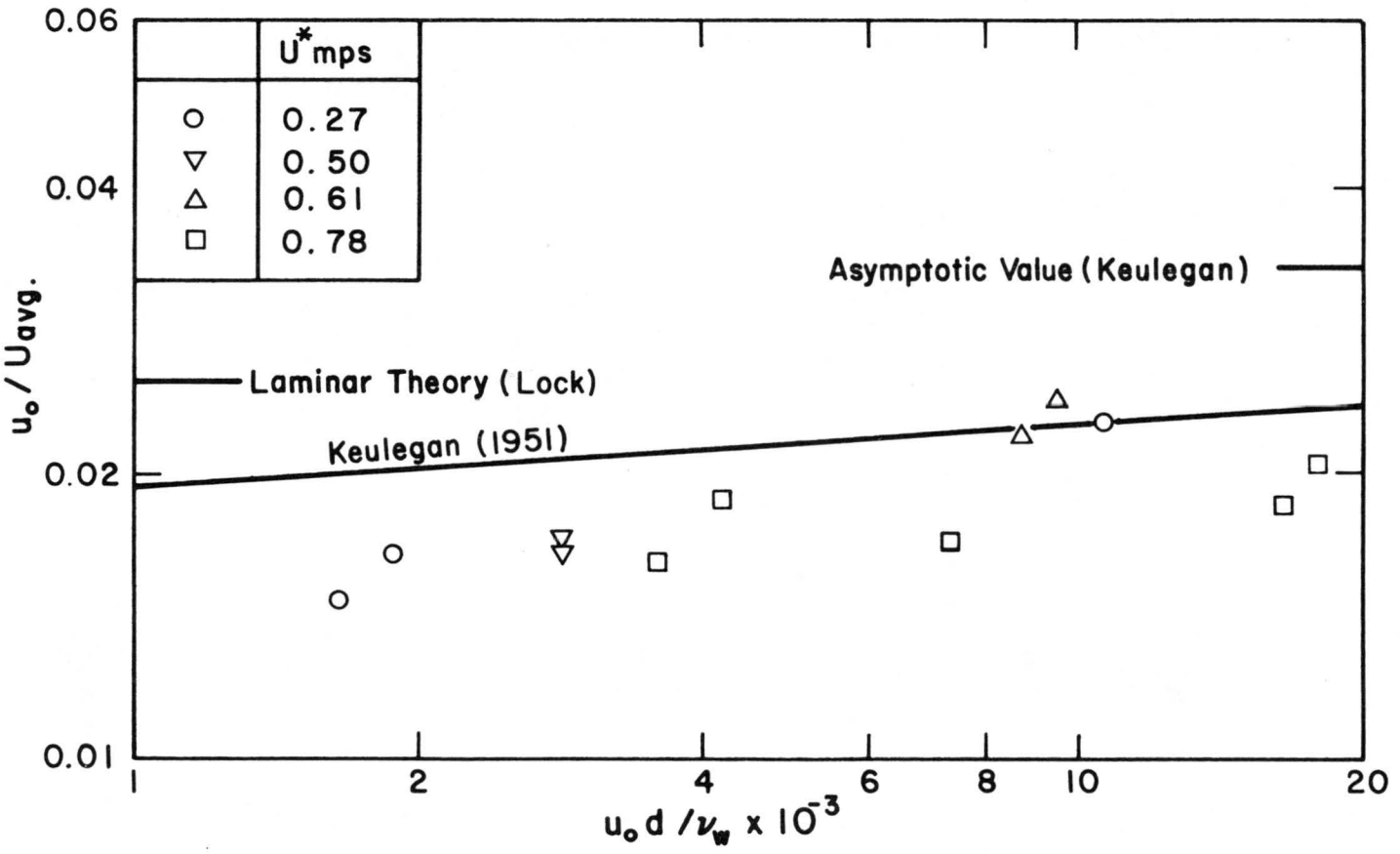
0.06
0.04
0.02
0.01
U* mps
0.27
0.50
0.61
0.78
Asymptotic Value (Keulegan)
Laminar Theory (Lock)
Keulegan (1951)
u_o / U_avg.
1
2
4
6
8
10
20
u_o d / ν_w x 10^-3

Figure 11

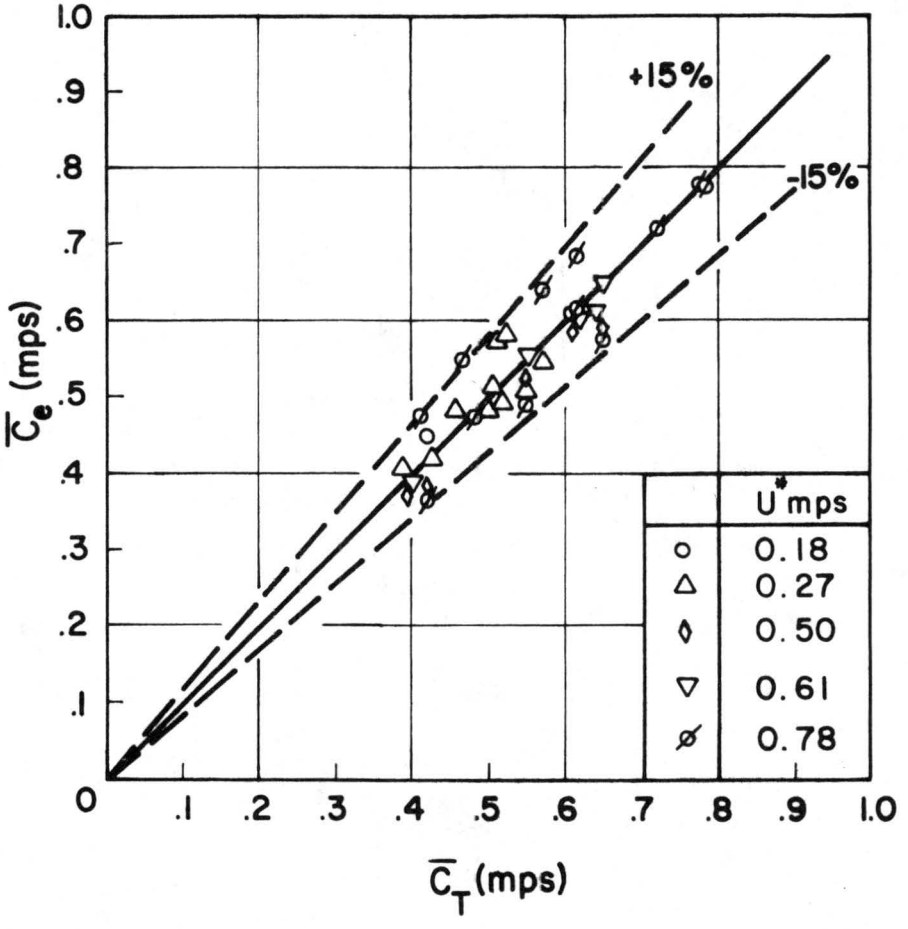
1.0
.9
.8
.7
.6
.5
.4
.3
.2
.1
0
.1
.2
.3
.4
.5
.6
.7
.8
.9
1.0
+15%
-15%
$\overline{C}_e$ (mps)
$\overline{C}_T$ (mps)
U* mps
0.18
0.27
0.50
0.61
0.78

Figure 12

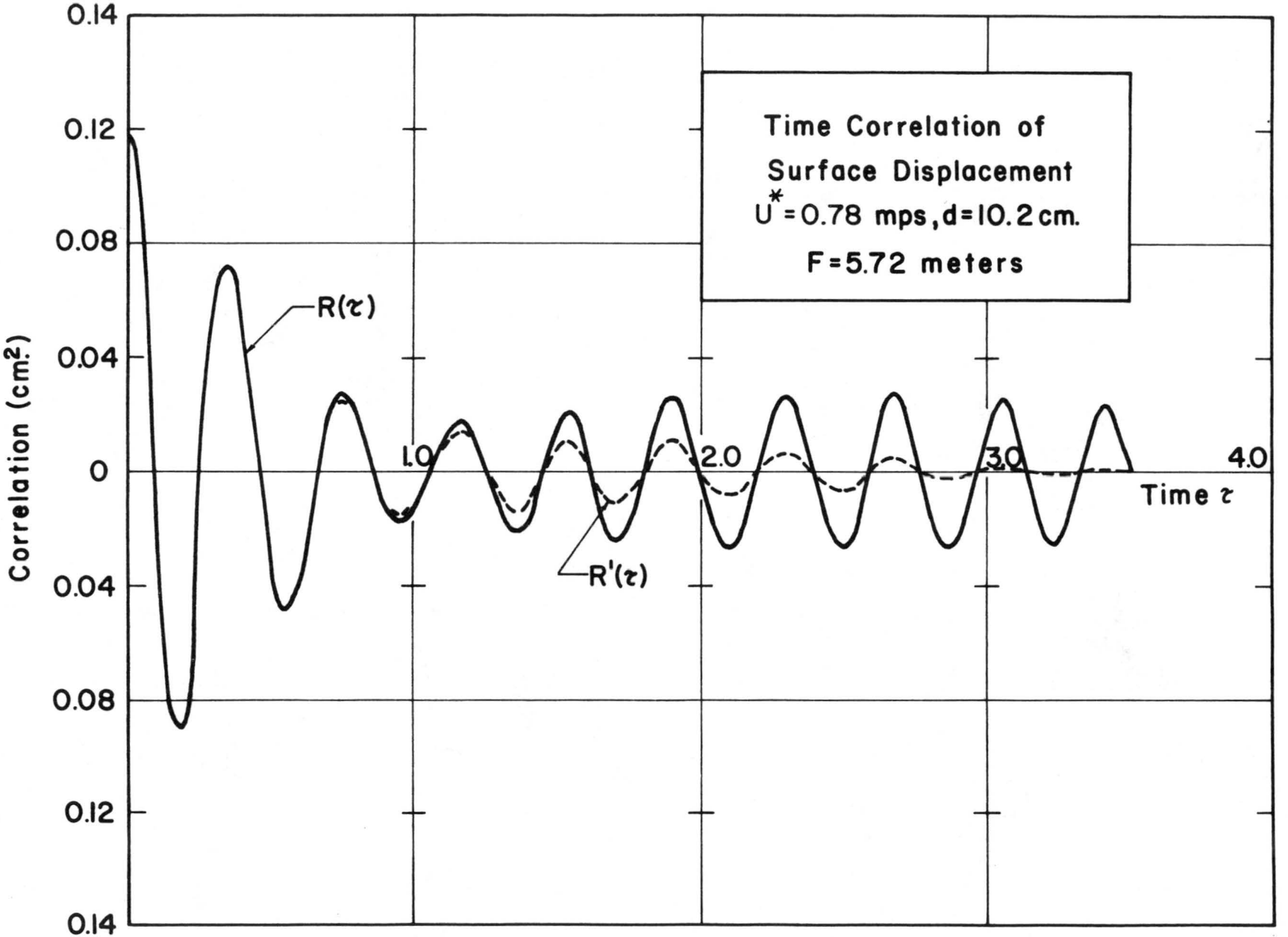
Time Correlation of
Surface Displacement
U* = 0.78 mps, d = 10.2 cm.
F = 5.72 meters
R(τ)
R'(τ)
Correlation (cm²)
Time τ
0.14
0.12
0.08
0.04
0
0.04
0.08
0.12
0.14
1.0
2.0
3.0
4.0

Figure 13

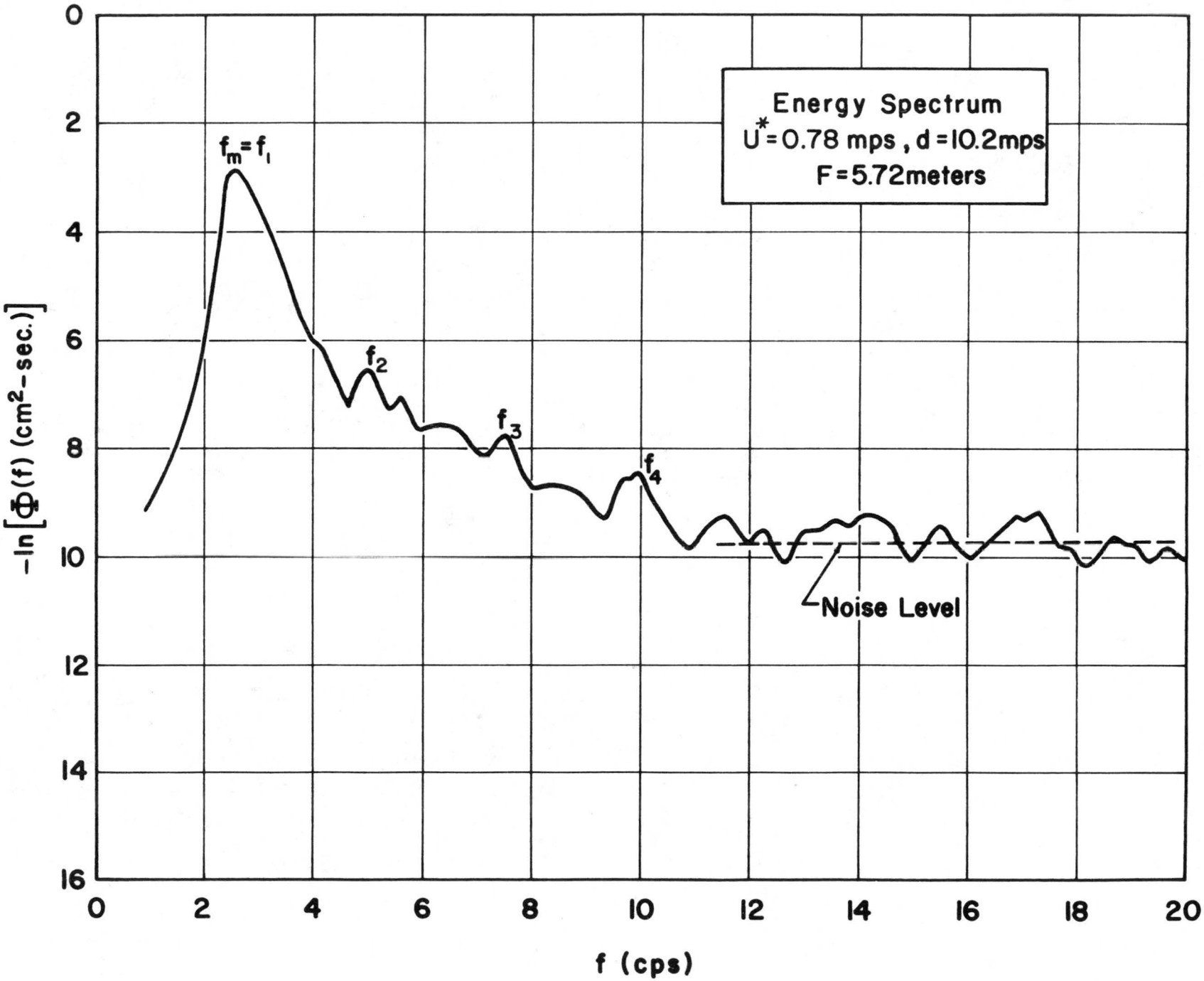
Energy Spectrum
U* = 0.78 mps , d = 10.2mps
F = 5.72meters
$f_m = f_1$
f_2
f_3
f_4
Noise Level
$-\ln[\Phi(f)\ (cm^2\text{-}sec.)]$
f (cps)
0
2
4
6
8
10
12
14
16
18
20

Figure 14

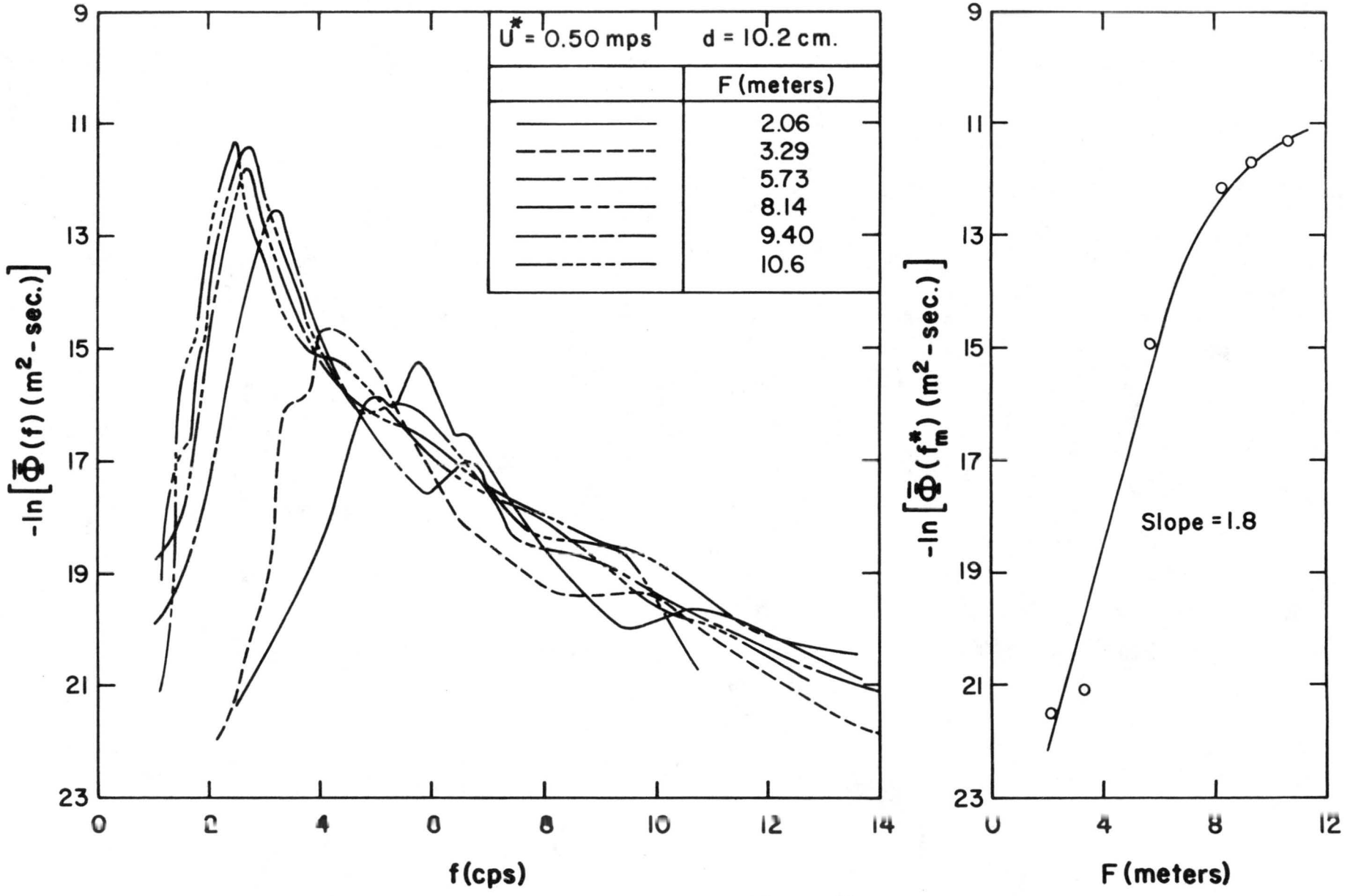
U* = 0.50 mps
d = 10.2 cm.
F (meters)
2.06
3.29
5.73
8.14
9.40
10.6
-ln [Φ̄ (f) (m²-sec.)]
f(cps)
-ln [Φ̄ (f*m) (m²-sec.)]
Slope = 1.8
F (meters)

Figure 15

A

B

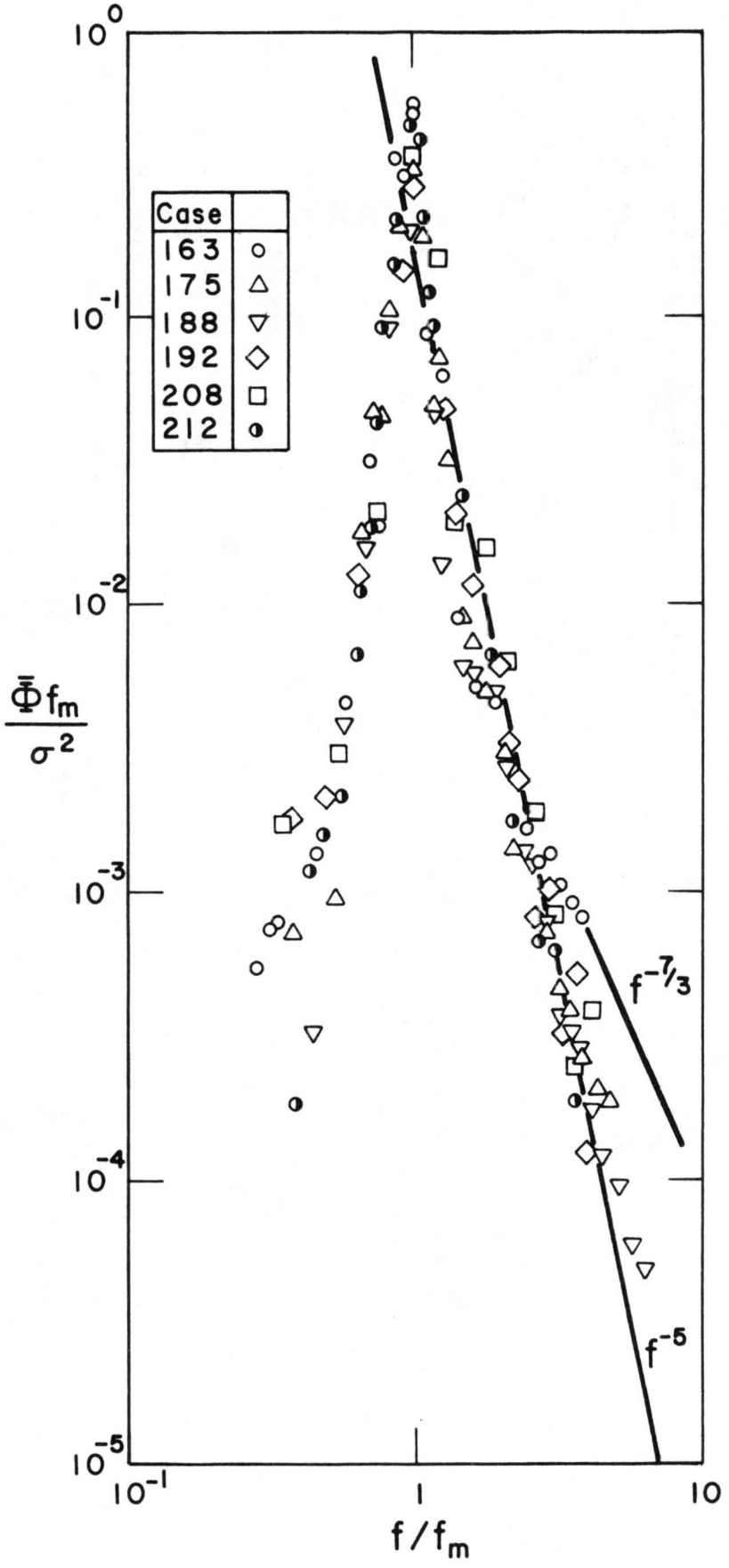
Case
163
175
188
192
208
212
10^{0}
10^{-1}
10^{-2}
10^{-3}
10^{-4}
10^{-5}
$\frac{\Phi f_m}{\sigma^2}$
$f^{-7/3}$
f^{-5}
10^{-1}
1
10
f/f_m

Figure 16